Experimental Thermal and Fluid Science 59 (2014) 166–183

Contents lists available at ScienceDirect

Experimental Thermal and Fluid Science

journal homepage: www.elsevier.com/locate/etfs

Flow boiling of R245fa in 1.1 mm diameter stainless steel, brass and copper tubes

E.A. Pike-Wilson, T.G. Karayiannis *

School of Engineering and Design, Brunel University London, Uxbridge, UB8 3PH, UK

ARTICLE INFO

Article history:
Available online 1 March 2014

Keywords:
Flow boiling
Microchannels
Surface characteristics

ABSTRACT

An experimental study of flow boiling heat transfer and pressure drop was conducted using R245fa in stainless steel, brass and copper tubes of 1.1 mm internal diameter. Experimental conditions include: mass flux range 100–400 kg/m^2 s, heat flux range 10–60 kW/m^2, pressure of 1.8 bar and exit vapour quality range 0–0.95. The tube surfaces were compared using scanning electron microscopy (SEM) and surface data acquired from confocal laser microscopy (CFLM), both showing differences between the surfaces. The heat transfer coefficient is similar in magnitude for all three materials but with a slight variation in trend. The heat transfer coefficient is seen to peak at high vapour qualities for stainless steel and brass, which is less evident with copper. The results were compared with past heat transfer correlations. These results showed better agreement with stainless steel compared to copper and brass. The pressure drop was shown to differ with surface characteristics, with the pressure drop for brass having a much steeper increase with heat flux. The pressure drop correlations tested did not show good agreement with the experimental results.

1. Introduction

In recent years, more research is being dedicated to understand flow boiling fundamentals in microchannels as a result of an increasing demand for cooling of high heat flux systems. With the reduction in channel diameter, the surface tension force dominates over gravity and thus new flow boiling characteristics can arise. Additionally, the effects of surface characteristics become increasingly important, Kandlikar [1]. Recently, Karayiannis et al. [2] presented flow boiling heat transfer rates in 1.1 mm seamless cold drawn and welded stainless steel tubes with R134a. The surfaces were analysed using scanning electron microscopy and were found to differ greatly. This resulted in differences in the heat transfer coefficient as a function of heat flux and local vapour quality. The effect of heat flux on the heat transfer coefficient was not clear for the welded tube and the trend with local vapour quality indicated sharp increases and decreases. In contrast, a clear heat flux effect was detected for the cold drawn tube, i.e. the heat transfer coefficient increased with heat flux and was constant with quality in the pre-dryout region. Flow visualisation showed differences in flow patterns at low heat fluxes [2]. They reported that surface characteristics could be one of the reasons for discrepancies in the results published by various research groups.

Differences in the inner surface characteristics of metallic tubes can be attributed to the material used (ductile versus hard) and the method of manufacture (cold drawn versus welded). Tubes that are either made of ductile materials or made by welding may have smooth surfaces whereas cold drawn seamless tubes made of hard material may have rough surfaces with many scratches. These scratches can act as cavities, which are important for bubble nucleation. Surface characteristics are also expected to affect the pressure drop when the flow is turbulent. The friction factor for laminar flow is a function of the Reynolds number while the turbulent friction factor is also a function of the pipe roughness. In microchannels, the largest contributor to pressure drop is friction, see [3], which will be affected by surface characteristics.

As mentioned above, surface effects are significant in flow boiling at the micro scale level [1,2]. However, surface parameters that are important need further clarification. Liu [4] investigated flow boiling heat transfer with stainless steel, brass and copper test sections and reported no significant effect of test section material. In a report published before [1], Kandlikar and Spiesman [5] reported a similar conclusion. They found that although the roughest surface (based on the average roughness) did perform generally better, there was no definite trend. Also, they concluded that the heat transfer performance was dependent on the number of cavities

* Corresponding author.
E-mail address: tassos.karayiannis@brunel.ac.uk (T.G. Karayiannis).

http://dx.doi.org/10.1016/j.expthermflusci.2014.02.024
0894-1777/

Nomenclature

Symbol

A	cross sectional area, m^2
C	chisholm constant
C_p	specific heat capacity, J kg^{-1} K^{-1}
D	diameter, m
f	fanning friction coefficient
Fp	floor distance to mean line, μm
G	mass flux, kg m^{-2} s^{-1}
h	specific enthalpy, J kg^{-1}
I	current, A
k	thermal conductivity, W m^{-1} K^{-1}
L	length, m
L_p	pressure drop length, m
M	molecular weight, kg $kmol^{-1}$
$\dot{m}$	mass flow rate, kg s^{-1}
N	number of samples
Na	active nucleation site density, –
P	pressure, Pa
Pr	Prandtl number
q	heat flux, W m^{-2}
Q_{loss}	heat loss, W
Q_v	heat generation rate per unit volume, W m^{-3}
Ra	average roughness, μm
Rp	maximum profile peak height (See Fig. 6), μm
Rq	root mean square deviation, μm
Rsm	mean spacing of profile irregularities (See Fig. 5), μm
Rt	maximum height, μm
Rv	maximum profile valley depth (See Fig. 6), μm
Rz	average maximum height, μm
T	temperature, °C
V	voltage, V
x	vapour quality
z	axial location

Greek symbols

α	heat transfer coefficient, W m^{-2} K^{-1}
β	percentage of data within ±30%
ε_{F_p}	equivalent roughness, μm
ΔP	pressure drop, Pa
λ_c	long wave component
λ_f	short wave component
μ	viscosity, N s m^{-2}
v	specific volume, m^3 kg^{-1}
ρ	density, kg m^{-3}
ϕ_L^2	two phase frictional multiplier

Subscripts

e	exit
Exp	experimental
f	fluid
fb	fluid bulk
g	gas
h	heated
i	internal
in	Inlet
l	liquid
LO	liquid only
m	measured
o	outside
Pred	predicted
sat	saturated
sp	single phase
sub	subcooled
tp	two phase
w	wall
wi	inner wall
wo	outside wall

Abbreviations

P	primary profile
R	roughness profile
W	waviness profile

and the cavity size distribution rather than the average roughness. Jones and Garimella [6] conducted experiments with deionised water in ten parallel channels to investigate the influence of surface roughness on heat transfer and pressure drop in microchannels. Three channels with average roughness values of 1.4, 3.9 and 6.7 μm were tested. The results showed little effect of surface roughness on boiling incipience, critical heat flux, wall superheat and heat transfer coefficient at low heat fluxes. However, at heat fluxes above 1500 kW/m^2, the two rougher surfaces gave different results with the heat transfer coefficient being 20–35% higher than that of the smoothest surface. The measured pressure drop was higher for the roughest surface. The study concluded that under certain circumstances, the surface roughness did have an influence on the flow boiling heat transfer coefficient and pressure drop. A study by Alam et al. [7] also concluded that the surface roughness has an influence on the heat transfer and pressure drop in flow boiling as well as on flow stability. This study used deionised water in silicon parallel channel heat sinks with gap dimensions of 500, 300 and 200 μm, with an original average surface roughness of 0.6 μm, which was further modified to 1 and 1.6 μm. Bubble nucleation site density and heat transfer coefficients were seen to increase with surface roughness but the pressure drop was not influenced. For the larger diameter heat sink, the inlet pressure fluctuations increased with surface roughness. However, the rougher surfaces did have a more uniform wall temperature. This was thought to be due to the higher nucleating bubble density, which led to a lower wall temperature. Zou and Jones [8] investigated the effect of heating surface material on subcooled flow boiling heat transfer. The study focused on how bubble dynamics, including the bubble growth rate and bubble departure size, the nucleation site density and the heat transfer coefficient changed for stainless steel and copper using R134a. They found that the heat transfer coefficient was affected by the material, although this had a minimal effect on the bubble dynamics. Copper was deemed to be the better material, giving higher heat flux values at a given wall superheat. This difference was attributed to the difference in thermal conductivities of the materials rather than the surface characteristics resulting from material changes.

A common problem faced by the research community when comparing surface characteristics is the method by which the surface characteristics are measured. Contact and non-contact measurements will differ due to the influence of the stylus. Another important factor is the way that the measurements are processed. The technique used for surface readings will affect the results, due to both the actual method of measurement and the standardisation of the method. For contact measurements using a stylus, the resolution of the surface readings are a function of the stylus dimensions. The tip of the stylus is run along the length of the surface,

with the readings based on the tip deflection. There are limitations to this method, relating to the size of the stylus which restricts access to small channels and the size of the smallest possible surface characteristics that can be detected. If the stylus is not able to enter into a cavity, it may give misleading results about the severity of the peaks. The stylus method may also lead to 'rounding' of cavities as corners cannot be entered by a rounded stylus tip. The use of optical techniques can give further details on the depth of these cavities without the limitation of the stylus radius. However, both of these processes have limitations in detecting true surface characteristics, which are important to flow boiling. Nucleation sites which are narrower at the surface but then increase in cross sectional area or volume, i.e. a re-entrant cavity, could not be detected by either technique [9]. Narrow but deep cavities may also not be detected due to the limitations of both contact and non-contact methods. If the cavity is at an angle, the stylus would not be able to enter and the cavity may not be detected. The angle of the laser, such as that used with confocal laser microscopy (CFLSM), to the surface would dictate how narrow cavities are detected. If the laser is not perpendicular to the cavity, it is possible due to laser scattering to give a false reading on the true depth of the cavity.

Roughness parameters are calculated after the waviness and profile (or form) are removed by filtering, see Fig. 1. The profile is the general shape of the surface. The surface will never be truly flat due to inaccuracies in machining or stress patterns. The waviness is a measure of the curvature of the surface due to the manufacturing process and this may be deliberate or due to process instability. The roughness is a measure of the smaller surface defects caused by cutting tools or the structure of the material [11]. The difference between the waviness and roughness values is a subjective matter, which is based on the application of the surface [12]. Filtering is a method of segregating the roughness, waviness and profile based on a certain wavelength and should allow an estimate of the actual surface roughness, not affected by surface waviness or profile. The smallest wavelength will be roughness as this is a finer surface detail and the surface profile will have the largest wavelength, see Fig. 1. Filtering is based on the transverse length, assessment (evaluation) length and sampling length (cut-off length), see Fig. 2. The cut-off is the length used for filtering and for identifying the irregularities characterising the surface [13] and is based on the measurements and the nature of the surface, not its geometrical properties [14]. It should also be based on the profile wavelength and not the evaluation length (see Fig. 2). The cut-off and the sampling length are not necessarily always the same [10], However, for roughness evaluation, see Fig. 2, these two parameters have the same value and are treated the same for the rest of this paper. The evaluation length should be approximately 5 times the cut-off, [11].

Depending on the method used for analysis and the type of filtering, one or two sampling lengths are removed from either end of the traverse length at the start of the analysis [11]. The traverse length should be 6–7 times greater than the cut-off length [15]. The wavelengths available for surface analysis are limited by the technique employed. As previously stated, the traverse and evaluation lengths, seen in Fig. 2, are a multiple of the cut-off but they are also in turn limited by the capability of the machine. For both contact and non-contact techniques, there is a maximum and a minimum distance that can be travelled as well as a limitation due to the actual physical length of the sample placed on the instrument. For example, a traverse length of 10 mm results in an appropriate cut-off of 1.4 mm. In the study of microchannel roughness, this is a large cut-off, which would not give an accurate representation of the finer surface characteristics.

Increasing the cut-off filter allows for a larger bandwidth to be classed as roughness instead of waviness and this will give inflated amplitude *Ra* values [16], see Fig. 3, where *Ra* is the arithmetic mean of the absolute ordinance across the sampling length (integral of roughness profile divided by length). As seen in the figure, the roughness values for the same surface decrease with the cut-off value. When the cut-off value is increased, more data is considered to be part of the roughness that may have previously been considered to be waviness. This will inflate the surface roughness values. On the other hand, a low cut-off can result in surface features being lost as only a small range of data is considered to be roughness.

Filtering is applied when processing the data, but the settings of the instrument when scanning will also affect the readings [18]. The resolution and scan size, the latter being the width along the scan, will have an impact on the readings. The surface is divided into a grid, with the measurements based on the average of each grid co-ordinate. The higher the number of grid co-ordinates set, the higher the resolution of the results. If the scan size is too large, then the grids will also be large and the resolution will be lower.

Surface parameters, are segregated into four groups, namely: amplitude, spatial, hybrid and functional parameters [11]. All these types include the roughness, R, waviness, W and primary profile, P, readings, see Fig. 1. The primary profile is the total profile with short wavelength filtering, which will remove noise and slanting when the readings are taken. The waviness and roughness profiles are both derived from the primary profile and are intentionally modified. The filters applied actually use multiple cut-offs to fully define the surface. This refers to the use of the Guassian filter,

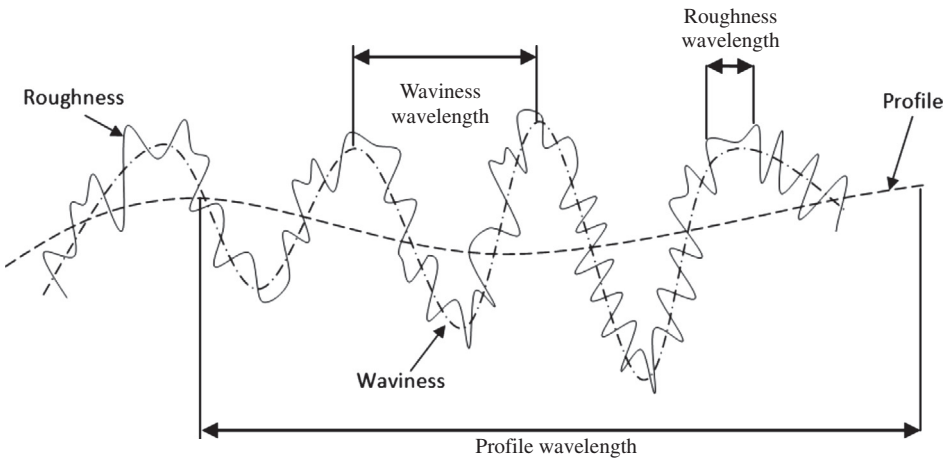

Fig. 1. Relationship between roughness, waviness and profile, adapted from [10].

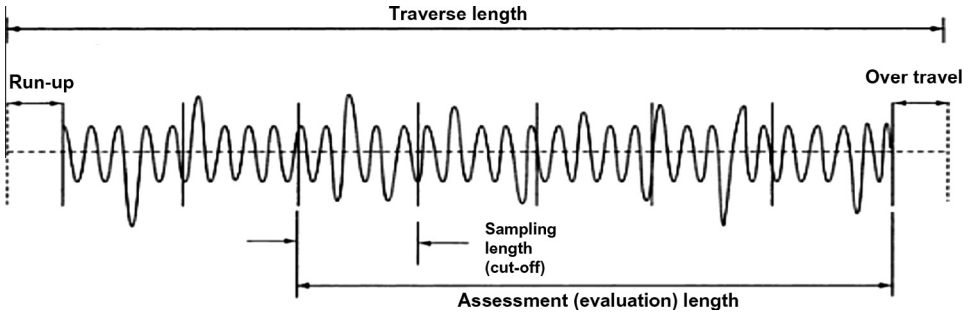

Fig. 2. Length definitions for surface measurements [11].

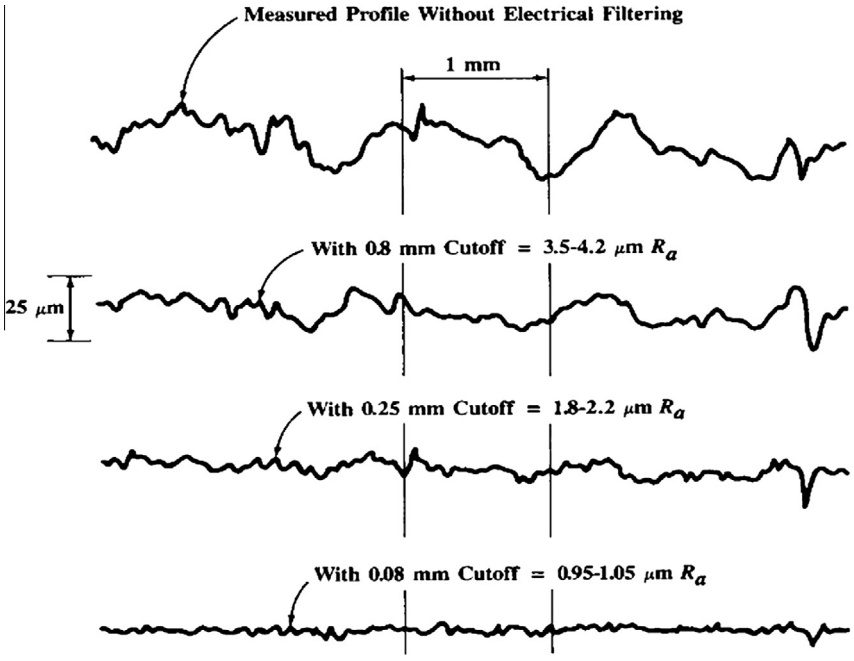

Fig. 3. The effect of various cut off values on average roughness, *Ra*, [17].

defined in ISO 11562-1996, where the filtering process requires a wavelength to be removed from the profile for parameters to be evaluated. The cut-off, which has previously been discussed, can be referred to as λ_c [15]. Recorded wavelengths below λ_c are classified as roughness and above as waviness. Further cut-offs include λ_f, which defines the boundary between the waviness and the profile. The waviness profile is found by removing λ_f and λ_c components. If only λ_f is removed, the roughness profile can be found. The effectiveness of a heat transfer surface has traditionally been compared using average surface roughness (*Ra*), an amplitude measurement, but it is now thought that this is not adequate for defining surface characteristics [10] and their effect on heat transfer rates since it allows for surfaces with different structures to have the same average roughness value, see Fig. 4.

Kandlikar and Schmitt [20] studied the effect of surface roughness on pressure drop in single phase flow and proposed three surface roughness parameters for characterisation of the surface, the maximum profile peak height, *Rp*, mean spacing of the profile irregularities Rsm (average of the Sm values) and the floor distance to the mean line, *Fp*, see Fig. 5. The floor profile mean line is the mean of all of the values, which fall below the main profile mean line. *Rp* and Rsm are predefined parameters from ASME B46.1-2002 [21] but *Fp* is a new parameter which is calculated from the 2D line plot data. Kandlikar and Schmitt [18] defined the equivalent roughness which can then be estimated from

$$\varepsilon_{F_p} = Rp + Fp \tag{1}$$

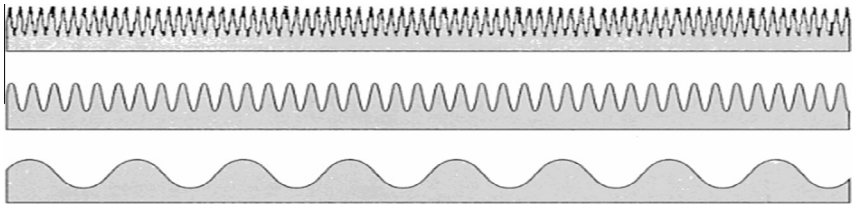

Fig. 4. Three distinctly different surfaces with the same average roughness value [19].

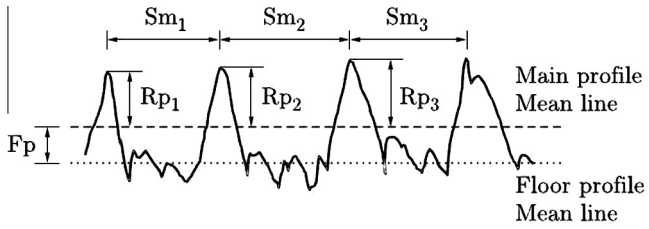

Fig. 5. Maximum profile peak height (*Rp*), spacing between irregularities (Sm) and floor distance to mean line (*Fp*), [20].

and can be used as an alternative to the average roughness. Young et al. [22] concluded that ε_{F_p} was a superior method of defining a surface when compared with average roughness, *Ra*. They found that many materials have a similar average roughness value but the ε_{F_p} values varied greatly.

There are three types of surface features, namely the profile peak (*Rp*) as above, profile valley (*Rv*) and profile elements, the latter is used to define Rsm, [23], see Figs. 5 and 6. The profile element is the length indicating where the profile, crosses the mean line, when changing in the same direction. The insignificant profile elements, usually caused by noise, for both the height and sampling length (see Fig. 2 for sampling length) need to be eliminated before the Rsm can be calculated. Profile elements with a height less than 10% of the *Rz* (average maximum height) and spacing of less than 1% of the sampling length are removed. *Rz* is *Rp* + *Rv* for the sampling length or the average maximum height [23], see Fig. 6. *Rz* is commonly used in pool boiling when defining a heater surface. Some may also use the "ten point" *Rz* value, which is similar to *Rz* but uses the average of the ten highest and lowest peaks and valleys of one of five sampling lengths. The final "ten point" value given is the average of all five samples [24]. O'Hanley [25] conducted a study into the effects of surface characteristics in pool boiling, characterising the surface as rough or smooth based on the "ten point" *Rz* values and the *Ra* values. For a smooth surface, $Ra < 0.1$ and $Rz < 1$ and a rough surface has $Ra > 1$ and $Rz \sim 15$. This study noted that if a surface comprises mainly of extrusions and not valleys, the *Rz* value will approach that of *Ra*. Therefore, the *Ra* and *Rz* values together give information about the structure of the roughness which the *Ra* value alone would not provide. As previously seen from Fig. 4, surfaces with different characteristics can have the same *Ra* values but they will differ in *Rz* value. The Rmax value, the difference in the maximum and minimum height across the profile, is also compared with *Rz*, where a similar value for *Rz* and Rmax suggests that the surface has one large peak or valley, which may be a surface flaw.

The present experimental study investigates flow boiling characteristics of R245fa using different metallic tubes, which have different surface characteristics. The experiments are conducted using stainless steel (Grade 304), brass (62% copper and 26% zinc) and copper (99% purity) tubes of 1.1 mm inside diameter. The surfaces of the test sections were compared using a SEM and with CFLM. Readings include the average surface roughness (*Ra*) and 2D profiles. Flow boiling heat transfer and pressure drop measurements were carried out. Experimental conditions include: mass flux range 100–400 kg/m^2, heat flux range 10–60 kW/m^2, inlet pressures of 1.8 and 2.4 bar and exit vapour quality range 0–0.95.

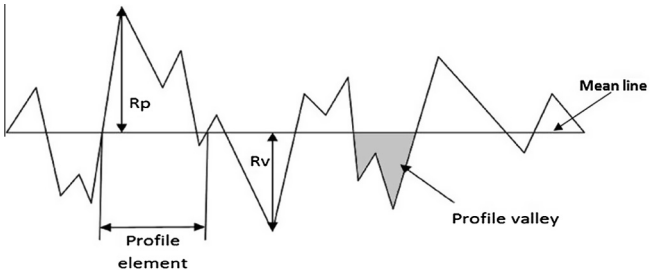

Fig. 6. Schematic diagram of a surface, representing the profile element and profile valley.

2. Experimental facility and procedure

The test facility was originally used to investigate the effect of channel diameter on flow boiling heat transfer using R134a [26]. The current experiments use R245fa as the working fluid to investigate the effect of channel material on flow boiling heat transfer and pressure drop in vertical tubes. Brass, stainless steel and copper test sections, all cold drawn seamless tubes of 1.1 mm internal diameter, are used. The internal channel diameter measurement has an uncertainty of 0.86–1.46%. A calming section is used to ensure that the flow is fully developed at the entry to the heated test section and the flow patterns are visualised through a borosilicate observation section using a high speed camera, which records 1000 frames per second with a resolution of 512 × 512 pixels. DC current is applied to copper electrodes at the inlet and outlet of the test sections for direct heating. A Yokogawa power meter WT110 (accuracy of 0.29%) is used to measure the supplied power. PTFE is used to electrically insulate the test section. Fourteen equidistance K-type thermocouples measure the outside wall temperature with a mean absolute error of ±0.23 K. The inlet and outlet fluid temperatures are measured using T-type thermocouples with an accuracy of ±0.18 K. Pressure transducers are used to measure the inlet and outlet pressures with an accuracy of ±1.5% and the pressure drop with an accuracy of ±0.08%. Fig. 7 presents a schematic diagram of the test section.

Temperature and pressure readings, captured via two data loggers and Labview, were recorded for 90 s and averaged to reduce random errors. Data were only recorded when the system was deemed to be at steady state, based on the oscillations in mass flow rate and temperature, see [2]. A single phase test is conducted at the start of each experiment to calculate the single phase Fanning friction factor (f) and the heat loss (Q_{loss}). The heat loss is calculated using a thermal loss coefficient (C_L), estimated during the single phase experiments and the average temperature difference across the insulation, see Eqs. (2)–(4). The inside temperature (T_{wJ}) and outside temperature ($T_{ins,0}$) of the heated section insulation is measured using K-type thermocouples. The calculated heat loss was used to calculate the heat flux to the tube wall, see Eq. (6).

$$\overline{\Delta T} = \frac{1}{N}\sum_{J=1}^{N} T_{wJ} - T_{ins,0} \tag{2}$$

$$C_L = \frac{VI - \dot{m}C_p(T_{out} - T_{in})}{\overline{\Delta T}} \tag{3}$$

$$Q_{loss} = C_L \overline{\Delta T} \tag{4}$$

In all subsequent experiments the heat loss is then obtained by measuring the $\overline{\Delta T}$ and multiplying by the loss coefficient.

$$f = \frac{\pi^2}{32}\frac{\rho_l \Delta P_m D_i^5}{\dot{m}^2 L_p} \tag{5}$$

$$q = \frac{\mathrm{VI} - Q_{\mathrm{loss}}}{\pi D_i L_h} \tag{6}$$

The local single phase heat transfer coefficient is given as:

$$\alpha_{\mathrm{sp}}(z) = \frac{q}{T_{\mathrm{wi}}(z) - T_{\mathrm{fb}}(z)} \tag{7}$$

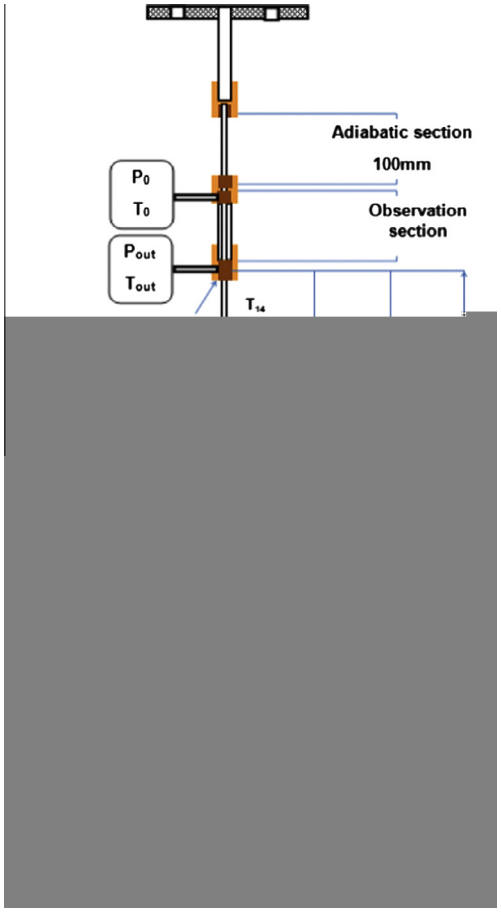

Fig. 7. Schematic diagram of the test section.

The internal local wall temperature is calculated from the steady state one dimensional heat conduction equation with internal heat generation, see Eq. (8), at specific locations, i.e. at the fourteen thermocouple points. The fluid temperature is calculated with an energy balance, Eq. (9).

$$T_{wi}(z) = T_{wo}(z) + \left(\frac{Q_v D_o^2}{16 k_w}\right)\left[1 - \left(\frac{D_i}{D_o}\right)^2 + \ln\left(\frac{D_i}{D_o}\right)^2\right] \tag{8}$$

$$T_{fb}(z) = T_{in} + \frac{q\pi D_i}{GAc_p} z \tag{9}$$

The local two phase heat transfer coefficient is based on the saturated temperature, see Eq. (10).

$$\alpha_{tp}(z) = \frac{q}{T_{wi}(z) - T_{sat}(z)} \tag{10}$$

The local saturated temperature is a function of the subcooled length and the local pressure. The pressure drop across the test section is assumed to be linear, see [27,28]. For a different approach, see also Bortolin et al. [29]. The subcooled length is found from iteration of Eqs. (11)–(15).

$$Z_{sub} = \frac{GAc_p(T_{sat}(z_{sub}) - T_{in})}{q\pi D_i} \tag{11}$$

$$\Delta P_{sp} = \frac{G^2}{\rho_L}\frac{2f}{D_i} z_{sub} \tag{12}$$

$$P(z_{sub}) = P_{in} - \Delta P_{sp} \tag{13}$$

$$\Delta P_{tp} = \Delta P_m - \Delta P_{sp} \tag{14}$$

$$P(z) = P(z_{sub}) - \frac{z - z_{sub}}{L_h - z_{sub}}\Delta P_{tp} \tag{15}$$

The local enthalpy is given by Eq. (16) and can be calculated from an energy balance and the inlet enthalpy, which is based on the local pressure (Eq. (15)). This in turn can be used to calculate the local vapour quality, Eq. (17).

$$h(z) = h_{in} + \frac{q\pi D_i z}{GA} \tag{16}$$

$$x(z) = \frac{h(z) - h_f(z)}{h_{fg}(z)} \tag{17}$$

The test section is directly heated with the voltage and current applied used to calculate the heat flux (Eq. (2)). The resistivity of brass and copper is lower than stainless steel. For example, a much lower voltage, 15 times lower, is applied for the same current with brass compared to stainless steel. Due to this, the maximum heat flux of brass and copper is lower than stainless steel. Therefore, a comparison of the two materials is based on a lower heat flux range than is possible with stainless steel. Also, the experiments for brass and copper were seen to be considerably more unstable at increasing heat flux, i.e. the inlet conditions became more difficult to control. Therefore the tests had to be stopped for copper and brass tubes before dryout at all mass flux values (100–400 kg/m^2 s) and high heat flux values (greater than 20 kW/m^2). Experiments with stainless steel were possible until dryout at mass fluxes of 100–300 kg/m^2 s, but were stopped before dryout for a mass flux of 400 kg/m^2 s, i.e. possible up to a heat flux of 30 kW/m^2.

The results were compared with correlations for both heat transfer and pressure drop. The comparison of correlations are based on the percentage of data (β) predicted within ±30% and the mean absolute percentage error (MAE) defined as

$$MAE = \frac{1}{N}\sum_{i=1}^{N}\frac{|h_{Pred,i} - h_{Exp,i}|}{h_{Exp,i}} \times 100 \tag{18}$$

The single phase experimental Fanning friction factor and Nusselt number were plotted against the Reynolds number and compared with known single phase relationships for both laminar and turbulent flow. The laminar single phase friction factor was compared with the laminar flow theory to good agreement, see Fig. 8. The uncertainty for the Reynolds number was calculated to be 15% on average, based on the method by Coleman and Steele [30]. The turbulent region was compared with Blasius [31] and Choi et al. [32]. The Choi et al. [32] correlation had better agreement with the brass and the Blasius [31] correlation better for stainless steel; both correlations had equally good agreement with the copper friction factor.

Fig. 9 represents the single phase Nusselt number compared with correlations from literature. The Choi et al. [32] correlation is for both laminar and turbulent flow but is seen to under predict the Nusselt number in the laminar region and over predict in the turbulent region for all materials. The Shah and London [33] correlation showed good agreement with the laminar Nusselt number. The correlations by Adams et al. [34], Gnielinski [35] and Petukhov [36] all over predicted with increasing Reynolds number. The Dittus and Boelter [37] correlations showed the best agreement for all the materials.

From Figs. 8 and 9, it can be concluded that the experimental methodology is suitable and the measurements are taken to a good accuracy. The maximum experimental uncertainty was calculated as 1.8% for the single phase and 8.4% for the two phase heat transfer coefficient. The uncertainty of the measured pressure drop is ±0.07%.

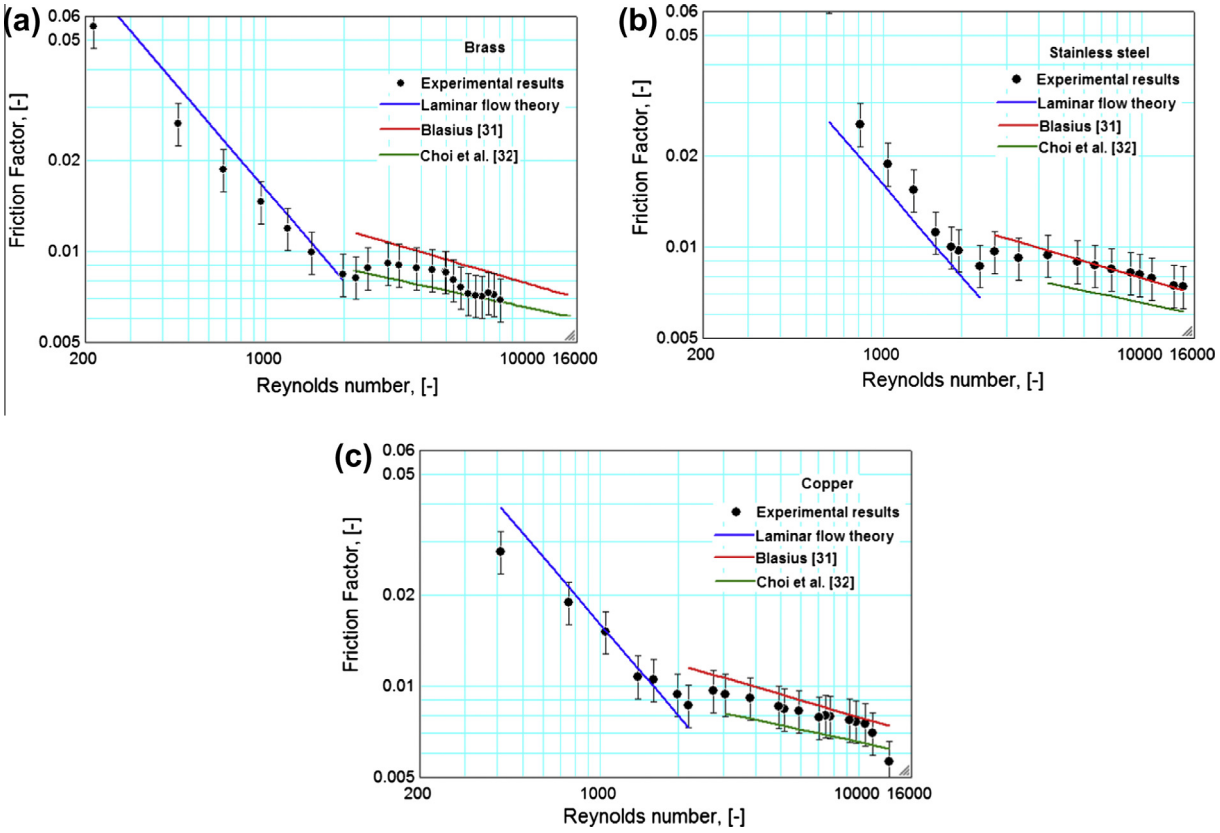

Fig. 8. Single phase friction factor as a function of Reynolds number for (a) brass, (b) stainless steel and (c) copper.

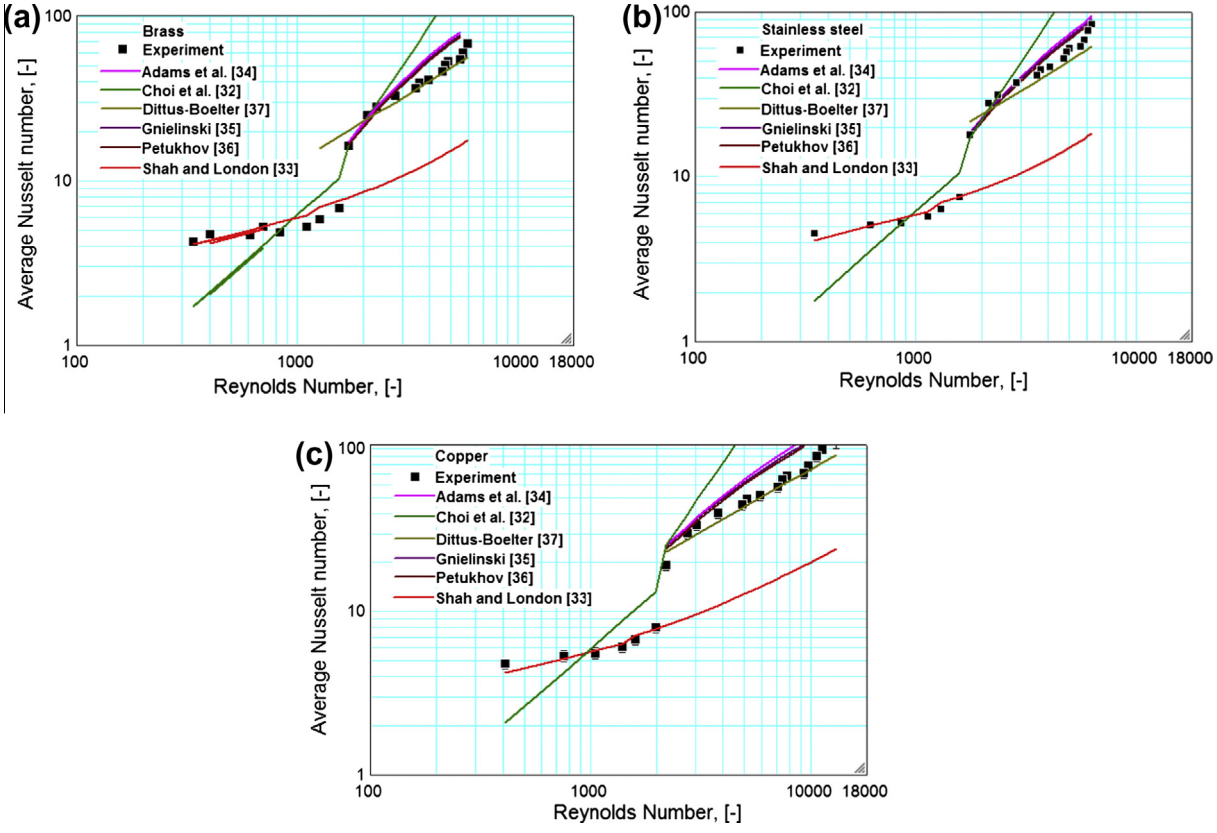

Fig. 9. Single phase Nusselt number as a function of Reynolds number for (a) brass, (b) stainless steel and (c) copper.

3. Results and discussion

3.1. Surface characteristics

The initial stage of surface comparison was to visually compare the surfaces using SEM and as seen in Fig. 10, the surfaces had different surface structures. To ensure that any imperfections were consistent with the material and manufacturing process, samples from different tubes were used for analysis. The surfaces were cleaned with acetone before scanning to remove any dirt, which may appear as surface imperfections. The SEM scans also allowed for a chemical analysis of the surface data to be done and this verified that the correct material was being used. The stainless steel surface is shown to have deposits on the surface but the results from the chemical analysis showed no foreign substance on the surface. These deposits were evident on all of the stainless steel samples, suggesting that they are a result of the manufacturing method. The brass surface has a flaky structure with horizontal cracks and surface imperfections. The copper surface has a smoother structure in comparison and does have 'stretches' from being cold drawn. All of the channels are seamless cold drawn but the surface characteristics as a result of this process differ between the materials.

The use of CFLM allowed for the average surface roughness and other surface parameters to be recorded, see Table 1 and the 2D profile of the surfaces depicted in Fig. 11. The primary profile (red line) is unaffected by the cut-off wavelength. Multiple cut-off wavelength filters were tested, showing a change in *Ra*, *Rp* and *Rt* of up to 30%. The surface roughness and the waviness will depend on the cut-off wavelength being applied. When a cut-off wavelength is set, any surface features with a wavelength larger than the cut-off will be classed as waviness and smaller classed as surface roughness. As mentioned earlier, the surface roughness can be seen as the fine detail of the surface [38]. The values for maximum profile peak (*Rp*) and maximum height (*Rt*) are higher for brass but this may be due to imperfections on the surface which bias the result, as can be seen in Fig. 9. Fig. 10b shows a greater variation in the surface profile for the stainless steel tube but a lower surface roughness. Since the surface roughness is a measure of the finer micro surface structure this leads to the conclusion that stainless steel has less variation in the micro structure than copper and brass, which can affect the shape and number of nucleation sites. In contrast to the findings of Young et al. [22], see introduction, there was a greater difference in average roughness values than equivalent roughness, i.e. ε_{F_p} for stainless steel and brass was calculated from Eq. (1) to be 2.9 μm and 2.4 μm for copper but the average roughness values were significantly different, with the brass values almost double that of stainless steel, see Table 1. All the roughness parameters compared (*Ra*, Rq, *Rp*, *Rv* and *Rt*) showed vast differences between the surfaces. As previously discussed, O'Hanley [25] used the *Ra* and the *Rz* value to characterise if the surface is rough or smooth. This method characterises the brass surface to be rough and the copper and stainless steel surfaces to be between smooth and rough.

3.2. Flow patterns

A dominating factor in both heat transfer and pressure drop are the prevailing flow patterns. The flow patterns were similar for all surfaces, with differences only at low heat fluxes. This is in agreement with Karayiannis et al. [2] who also found the only variance in flow patterns between tubes with different manufacturing methods – cold drawn and welded – to be at low heat fluxes. Their work concluded that these differences were due to the welded tube being much smoother with only some anomalies or debris distributed non-uniformly along the tube. These may or may not act as nucleation sites (depending on location and shape). Hence nucleation in the welded tube may commence at a smaller number of locations compared to the cold drawn stainless steel tube described in [2] which has uniform scratches along the tube – hence more possible nucleation sites.

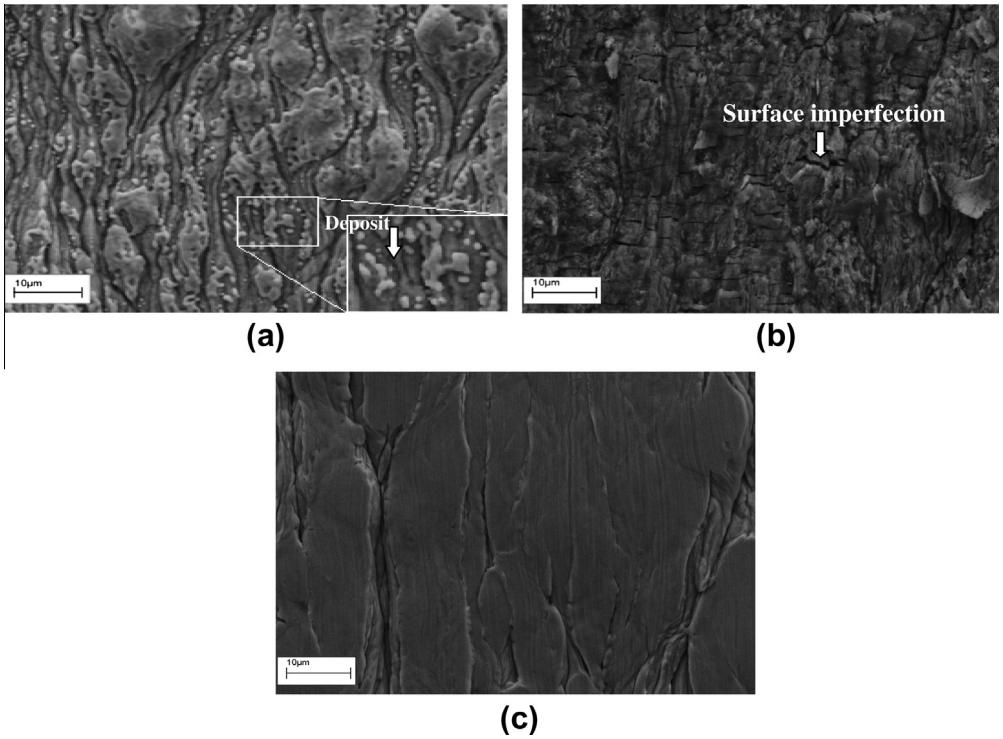

Fig. 10. SEM results for (a) stainless steel (b) brass and (c) copper at a magnification of 5000.

Table 1
Surface parameter readings for stainless steel and brass with a 0.025 mm cut off.

Material	Average roughness, *Ra* (μm)	Root mean square deviation, Rq (μm)	Max profile peak height, *Rp* (μm)	Lowest point from Mean Line, *Rv* (μm)	Maximum height, *Rt* (μm)	ε_{F_p} (μm)
Brass	1.249	1.743	5.465	6.409	11.874	2.9
Stainless steel	0.716	0.928	2.109	2.992	5.248	2.9
Copper	0.524	0.722	2.406	2.260	4.666	2.4

The dominant flow pattern for all three test sections was annular flow. The flow patterns were based on the classifications by [39] of bubbly, slug, churn and annular flow. For the copper and brass test section, slug flow was briefly seen at low heat fluxes before becoming churn flow and annular flow. Only annular flow was seen for the stainless steel test section even at the low heat fluxes tested, see Fig. 12. Based on an inlet pressure of 1.85 bar and a mass flux of 300 kg/m^2 s, annular flow was seen at a heat flux of 7.8 kW/m^2 in comparison with 8 kW/m^2 for copper and 10 kW/m^2 for brass. Slug flow was not seen as frequently at the higher inlet pressure of 2.45 bar for copper but was still present in brass.

The above flow patterns relate to the heat flux being increased. Interestingly, when the heat flux was decreased, the full range of flow patterns were observed. Fig. 13 shows these flow patterns in terms of the heat flux and vapour quality for the stainless steel test section at a pressure of 2.45 bar and a mass flux of 300 kg/m^2 s. As with the increasing heat flux, the heat fluxes at which these flow patterns were observed varies with the tube material. Bubbly flow

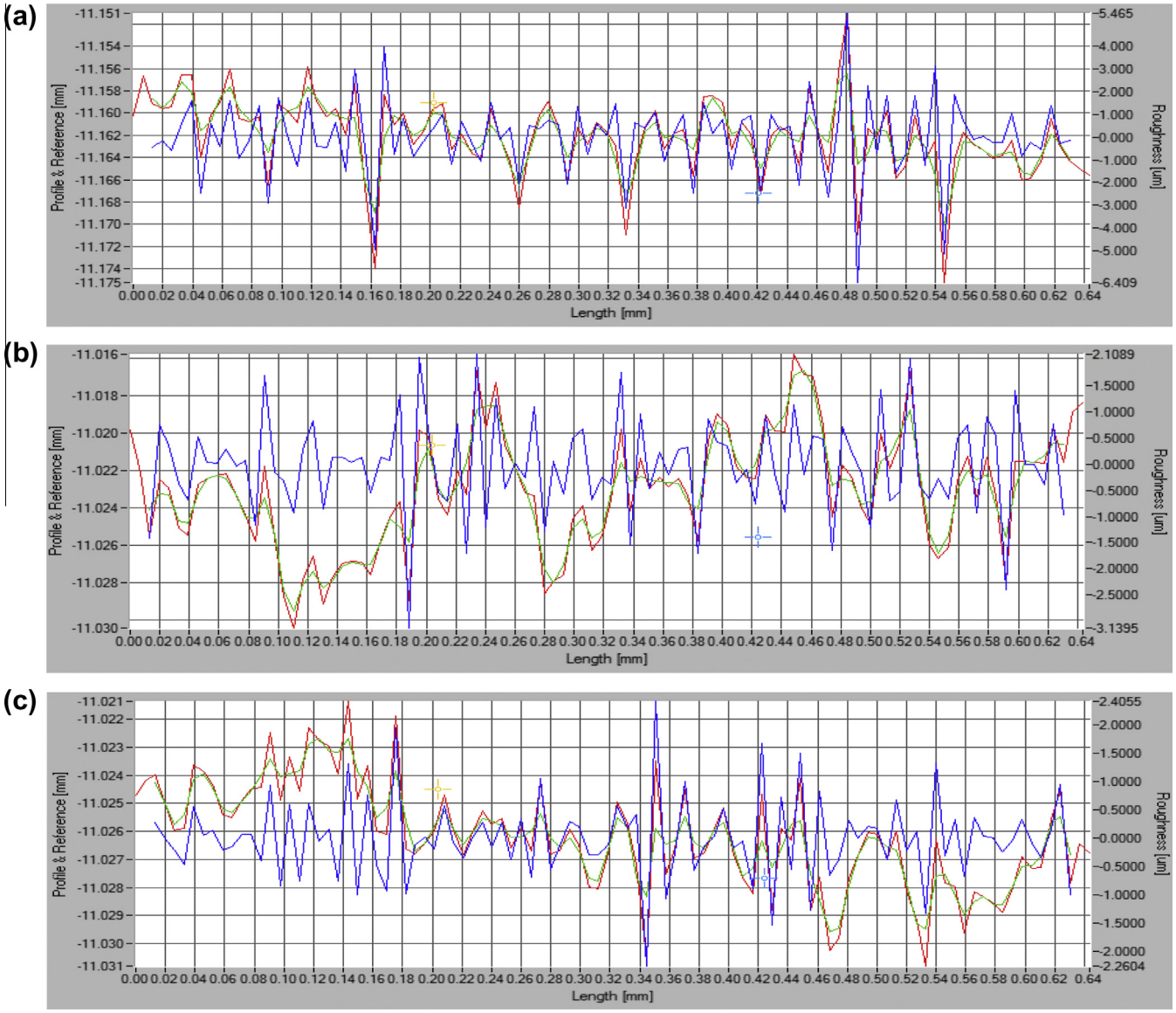

Fig. 11. 2D profile of (a) brass, (b) stainless steel and (c) copper surface with a 0.08 mm cut-off (Red line: profile, green line: waviness and blue line: roughness. The Profile and Reference used for the axis is a nominal value based on the distance of the laser from the surface and is not used as part of the analysis). (For interpretation of the references to colour in this figure legend, the reader is referred to the web version of this article.)

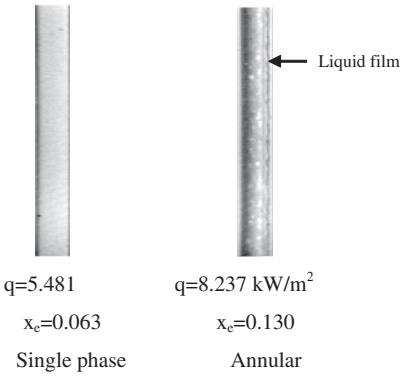

Fig. 12. Flow patterns for R245fa at G = 300 kg/m^2 s and T_{sat} = 31 °C, with increasing heat flux in the stainless steel test section.

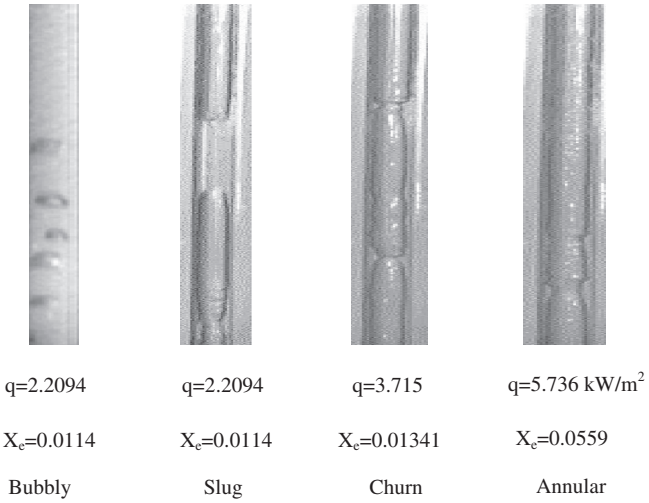

Fig. 13. Flow patterns for R245fa at G = 300 kg/m^2 s and 1.85 bar, with decreasing heat flux in the stainless steel test section.

was only seen at the lowest heat fluxes for all three materials. The flow patterns seen in Fig. 13 were observed for all of the materials, across the whole range of pressure, mass flux and heat flux.

3.3. Pressure drop

The measured pressure drop increased with heat flux and mass flux, see Fig. 14. Brass has a higher measured total pressure drop, with a much steeper increase with heat flux for two phase flow. The effect of mass flux on pressure drop is less in the brass tube than in the stainless steel and copper tube for the range studied. This suggests that surface characteristics do have an effect on the two phase pressure drop. Although the roughest surface, brass, has the highest pressure drop, there is no clear trend between the two phase pressure drop and average surface roughness. As seen in Fig. 15, brass has the highest measured pressure drop. It can be noted that the maximum heat fluxes seen in Fig. 15 occur at different exit vapour qualities, mainly due to the experiments being stopped for copper and brass due to instabilities. The exit vapour quality is highest for stainless steel, at 1, compared with 0.56 for brass and 0.39 for copper.

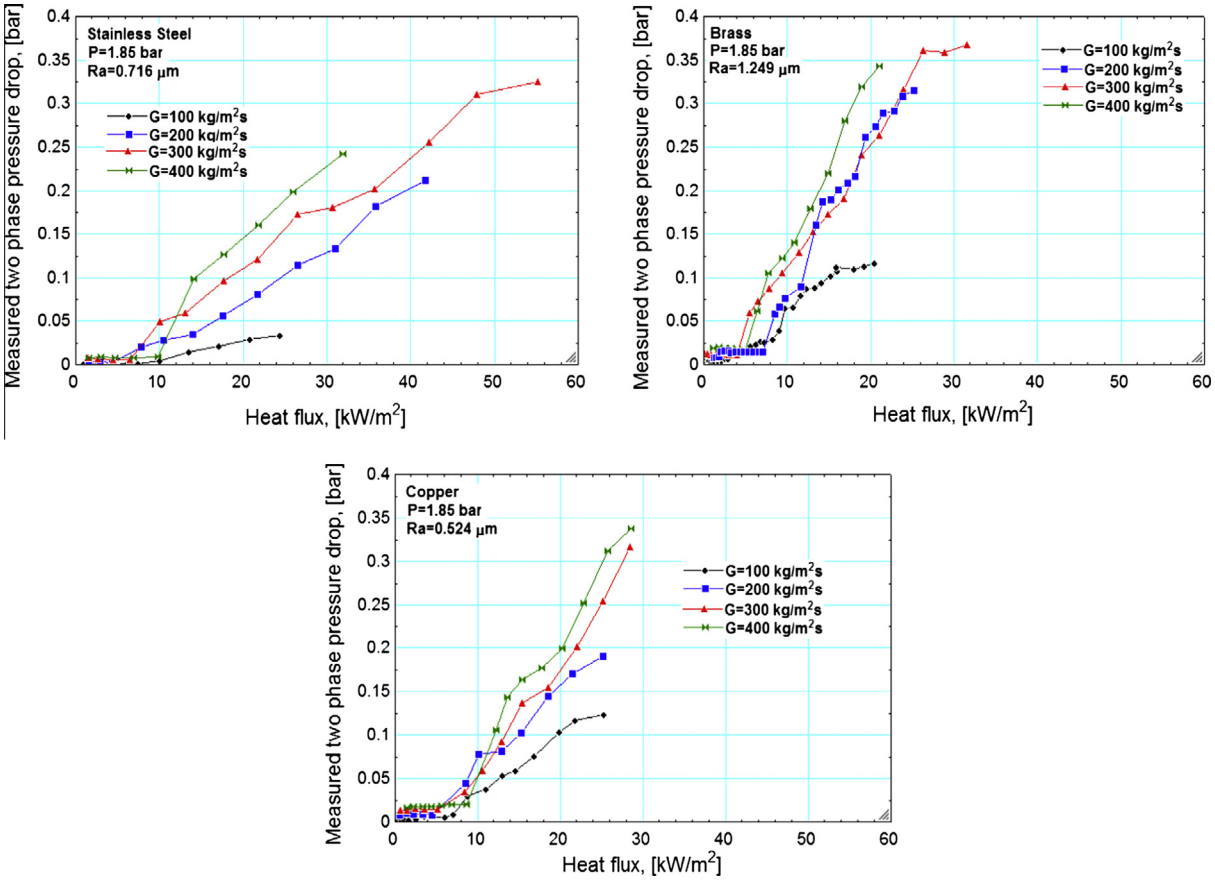

Fig. 14. Effect of mass flux on pressure drop for stainless steel, brass and copper at P = 1.85 bar.

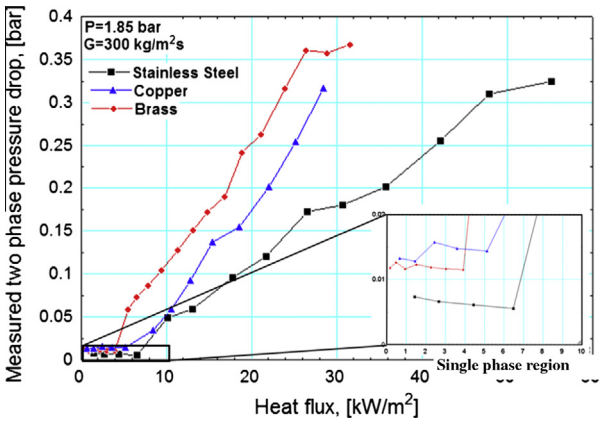

Fig. 15. Pressure drop for stainless steel, brass and copper at $P = 1.85$ bar and $G = 300$ kg/m^2 s.

The total pressure drop is the summation of frictional, gravitational and acceleration components. A comparison demonstrated that the percentage that each component contributed was very similar for all tubes, i.e. the greatest contributor is friction, responsible for approximately 85% of the pressure drop at higher vapour qualities. Some differences occurred only at small exit vapour qualities, i.e. acceleration contributes a higher percentage of the pressure drop for stainless steel at vapour qualities less than 0.1.

The experimental data was compared with predicted data from pressure drop correlations. None of the correlations showed satisfactory results for any tube material, see Table 2. This was expected due to the large pressure drops recorded for this refrigerant compared to for example R134a [40]. Note that this refrigerant was not included in the data bank used to obtain any of these correlations. There was no one correlation which was the best for all three materials. Lockhart and Martinelli [41], which is a macroscale correlation, performed better across three materials. Generally, the predictions for copper are the worst even though the predicted measured pressure drop falls in the middle of the three materials, see Fig. 15. The correlation of Zhang et al. [42] and the homogenous model also performed well for all three materials. The frictional component of the pressure drop for the homogenous model is based on the liquid only friction factor which is similar for all the tubes, see Eq. (19) [43].

$$\phi_{LO}^2 = [1 + x(\upsilon_{fg}/\upsilon_f)][1 + x(\mu_{fg}/\mu_g)]^{-\frac{1}{4}} \tag{19}$$

The remaining pressure drop correlations use a function of X to define the two phase frictional multiplier, where X is calculated from:

$$X = \left(\frac{f_L}{f_g}\right)^{0.5}\left(\frac{\rho_g}{\rho_L}\right)^{0.5}\left(\frac{1-x}{x}\right) \tag{20}$$

This includes a function of the liquid and vapour friction factor, which vary greatly between the tubes, mainly due to the difference in the measured pressure drop. The friction factors are calculated based on the laminar flow theory and the Blasius [31] equation. The Reynolds numbers are calculated from Eqs. (21) and (22), for the liquid and vapour regions respectively.

$$Re_L = \frac{(1-x)GD_i}{\mu_f} \tag{21}$$

$$Re_G = \frac{GxD_i}{\mu_g} \tag{22}$$

The two phase pressure drop is predicted based on the single phase prediction multiplied by a two phase frictional multiplier, which is mainly based on the fluid properties and is different for each correlation. For example, the frictional pressure drop for the homogenous model can be calculated from Eq. (23) but for the Lockhart and Martinelli [41] the frictional pressure drop is calculated from Eq. (24).

$$\Delta P_f = \frac{2f_{LO}LG^2}{D\rho_L}\left[1 + \frac{x_e}{2}\left(\frac{\rho_L}{\rho_{fg}}\right)\right] \tag{23}$$

$$\Delta P_f = \frac{L}{x_e}\int_0^{x_e}\frac{2f_L G^2}{D\rho_L}\phi_L^2 dx \tag{24}$$

where ϕ_L^2 is calculated using Eqs. (20) and (25) respectively.

$$\phi_L^2 = 1 + \frac{C}{X} + \frac{1}{X^2} \tag{25}$$

The Lockhart and Martinelli [41] correlation uses a set value of the Chishom constant, C, to calculate the two phase frictional multiplier based on whether the gas and liquid is in a laminar or turbulent state. The Zhang et al. [42] is based on fluid properties and channel diameter, the latter being the same for all channels. The data predicted within ±30% is notably better for stainless steel than brass and copper with the Lockhart and Martinelli [41] and Zhang et al. [42]. Zhang et al. uses the Laplace constant which includes surface tension and density, both of which will change with heat flux. Figs. 17 and 18 represent the predictions of the Lockhart and Martinelli [41] and the Zhang et al. [42] correlations at both inlet pressures. These graphs represent the results for the best performing macro scale and micro scale correlations respectively. It can be seen that there is no improvement in prediction with the micro scale correlation. The effect of inlet pressure on the measured pressure drop was most evident for stainless steel at high heat fluxes which showed up to 30% difference, as opposed to brass which demonstrated minimal difference, see Fig. 16. A difference was seen with copper but only at the highest heat fluxes. Although the pressure drop correlations include a function of mass flux, this does not account for the increase in

Table 2
Comparison with pressure drop correlations.

Correlation/model	Stainless steel		Brass		Copper	
	β %	MAE %	β %	MAE %	β %	MAE %
Mishima and Hibiki [45]	6.3	81.0	13.8	219.5	8.1	149.9
Lockhart and Martinelli [41]	45.8	37.1	21.9	95.3	18.2	24.1
Zhang et al. [42]	40.5	35.6	16.2	74.6	14.1	42.8
Homogenous model	35.4	36.6	26.8	28.8	17.2	33.9
Warrier et al. [46]	0	206.2	17.8	84.3	10.1	43.2
Qu and Mudawar [47]	31.6	118.4	23.6	55.4	20.2	22.3
Li and Wu [48]	5.1	103.1	21.9	141.9	18.2	14.5
Yu et al. [49]	21.5	49.5	14.6	107.4	15.2	110.4
Lee and Garimella [50]	29.1	73.0	17.1	39.9	18.2	24.9
Del Col et al. [44]	2.5	41.6	13.9	68.6	39.5	4.1

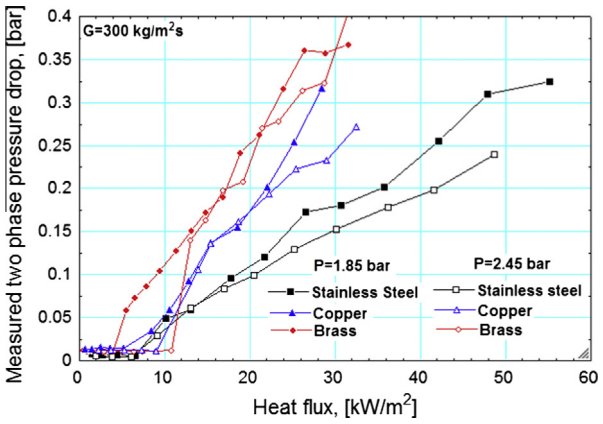

Fig. 16. Effect of inlet pressure on measured pressure drop for stainless steel, copper and brass at pressures of 1.85 and 2.45 bar.

pressure drop with mass flux seen here and the correlations perform worse as the mass flux increases. Only one pressure drop correlation includes the effect of the surface characteristics, Del Col et al. [44]. This correlation uses the relative roughness of the channel, RR, which is calculated from Eq. (26).

$$RR = \frac{2Ra}{D} \tag{26}$$

Although this correlation showed varying results for the different materials, the predicted pressure drop was over predicted and showed poor agreement with the experimental results. The highest predicted pressure drop is that of copper, followed by stainless steel and then brass. This does not follow the same trend as the measured pressure drop and is the reverse trend of the average roughness values. Brass showed the best agreement, with 25.4% of the data predicted within ±30% with a mean absolute percentage error of 77.3%. The worst performing was stainless steel, with a β value of 1.3%, where the measured pressure drop is the lowest. Del Col et al. [44] noted that this correlation over predicts at low liquid only Reynolds numbers, which is seen here where the experimental data is at low liquid only Reynolds numbers.

3.4. Heat transfer

The flow boiling heat transfer results are compared based on plots of the heat transfer coefficient versus local vapour quality and axial location for different heat flux and mass flux values. It can be seen that the magnitude and the trend of the local heat transfer coefficient is similar for both stainless steel and brass, see Figs. 19 and 20.

However, the heat transfer coefficient curve is smoother for brass than stainless steel, which has peaks. These peaks are thought to be the result of surface flaws or scratches, which can form nucleation sites. This can be inferred based on the fact that these peaks in heat transfer coefficient values are seen only after nucleation occurs. Also, when the heat transfer coefficient is plotted as a function of axial location, it is clear that the peaks occur at the same axial location for all heat fluxes and mass fluxes again indicating a local surface characteristic or flaw/scratch resulting in higher local heat transfer coefficients, see Fig. 20a. The fact that the results for the two tubes are similar (except the local peaks of course) are in agreement with Liu [4] who found no significant difference in the trend or magnitude of the local heat transfer rates between stainless steel and brass. The heat transfer coefficient of copper does not show the same increasing trend as with brass and stainless steel, with only a small increase at the tube exit. In general, the heat transfer over the tube length is lower for copper than that of the other two materials, see Fig. 21.

Fig. 21 shows that at low vapour qualities, $x < 0.35$, there is no clear effect of surface characteristics. At higher vapour qualities, the roughest surface has the highest heat transfer and the smoothest has the lowest. This is not seen across the whole mass flux and pressure drop range, which is in agreement with Jones et al. [6], i.e. surface characteristics may be important in certain circumstances or ranges. The onset of nucleate boiling can clearly be seen for copper, with a jump in the heat transfer coefficient. For the higher pressure, this point occurred at a lower heat flux for copper when compared with the stainless steel and brass tubes, where the onset of nucleate boiling occurred at higher but similar heat fluxes. Copper, being the smoothest surface, has the lowest heat transfer coefficient for all mass fluxes and heat fluxes tested. One would expect the highest heat transfer coefficient to occur in the roughest tube, i.e. the brass test section. However, this is not exactly the case for the entire range of heat and mass fluxes studied. For certain values of the above quantities, the heat transfer coefficient is higher in the brass tube compared to the stainless steel tube but for a different range of values the opposite is true. Unfortunately, we could not detect, at this stage, a trend when trying to access this complex dependency of the heat transfer coefficient on mass and heat flux in relation to surface roughness (Ra).

Fig. 22 shows the boiling curve at an axial location of 0.075 m, representing the entry region of the tube. It shows that the onset of nucleate boiling occurs at similar heat fluxes for copper and stainless steel. Flow observation with these measurements showed differences in the flow patterns observed at the exit of the tube at the onset of nucleate boiling. For the copper tube, slug flow was

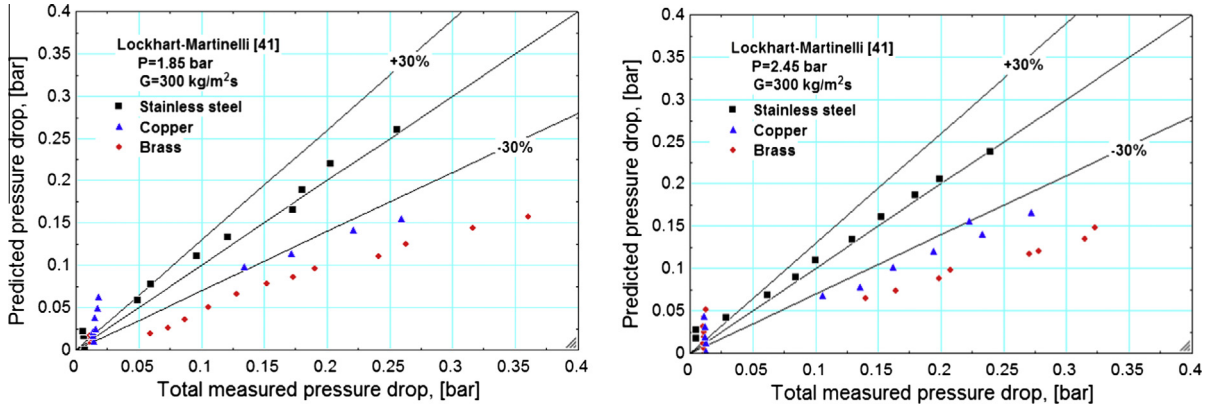

Fig. 17. Comparison of the experimental results and the Lockhart and Martinelli [41] correlation for stainless steel, copper and brass.

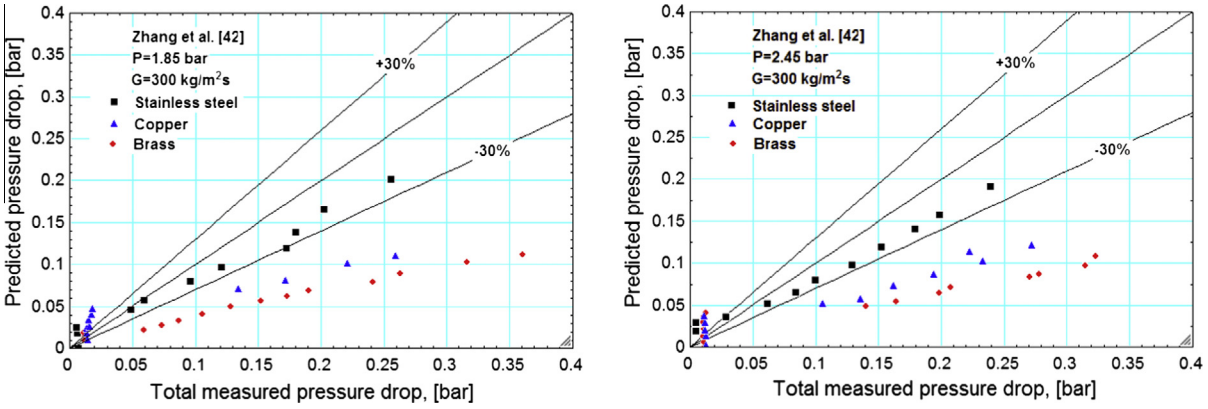

Fig. 18. Comparison of the experimental results and the Zhang et al. [42] correlation for stainless steel, copper and brass.

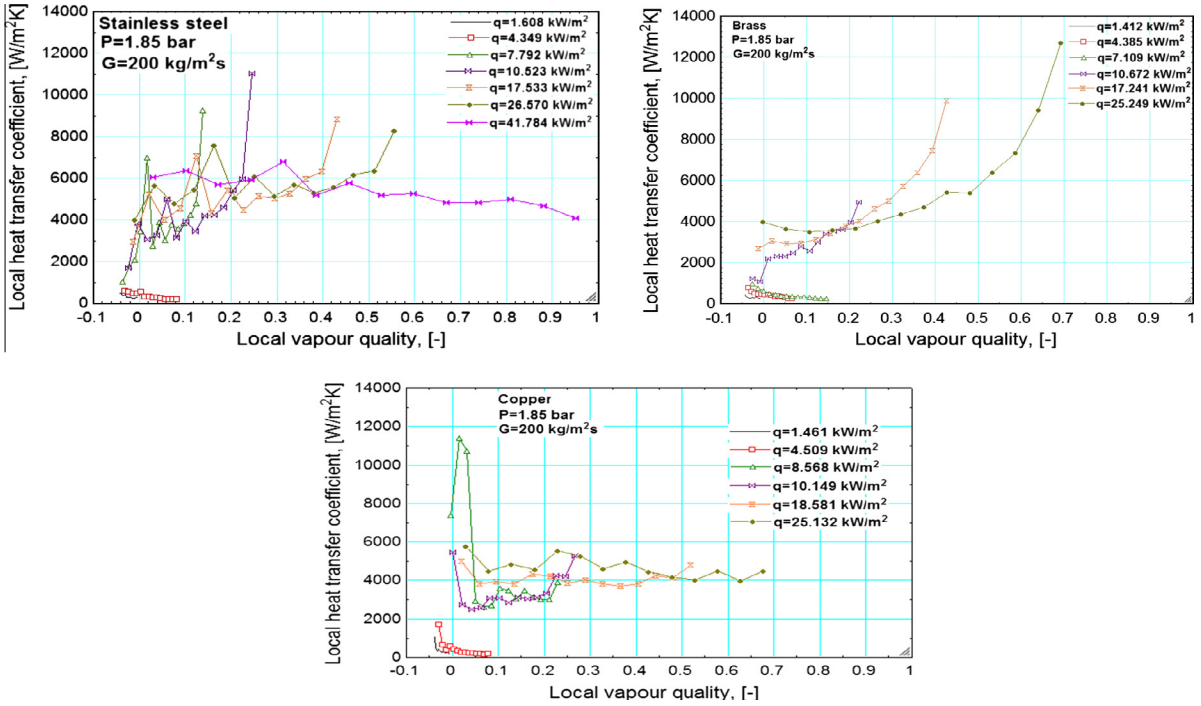

Fig. 19. Local heat transfer coefficient for stainless steel, brass and copper at an inlet pressure of 1.85 bar and mass flux of 200 kg/m^2 s.

observed at this point, indicating a transition from nucleation to slug flow occurred within the tube. Annular flow was evident for stainless steel where all other conditions were the same indicating that the surface may have an effect on flow transitions.

The onset of nucleate boiling occurs at a higher heat flux and greater wall superheat for brass. After the onset of nucleate boiling, the wall superheat is lowest for stainless steel and brass remains at the highest wall superheat. Wall superheat is related to the surface characteristics in terms of the size of the active nucleation sites [51]. Larger nucleation sites require a smaller wall superheat to active, suggesting that brass has smaller nucleation sites which require a higher wall superheat to activate. Cornwell and Brown [52] found the relationship between the wall superheat and the active nucleation site density for pool boiling to be:

$$Na \sim \Delta T_w^{4.5} \tag{27}$$

Based on the above equation, brass would have a highest number of active nucleation sites and copper the lowest. This trend is in agreement with the average surface roughness values. There is approximately 30% difference between the average roughness values and the wall superheat for stainless steel and copper. Brass is over 200% higher in average roughness values and wall superheat. This suggests that there is some dependence on the average roughness but this can only be verified by a comparison over a wider range of average roughness values.

Zou and Jones [8] concluded that the nucleation site density correlated well with the surface heat flux. They also found copper to have a lower wall superheat at a given heat flux and a better heat transfer performance in comparison with stainless steel. The similarity between the two materials in terms of nucleation site density, bubble departure size and growth rate led them to state that the differences in the heat transfer between the surfaces were due to the thermal conductivity and not surface characteristics. Copper has a much higher thermal conductivity compared with stainless steel, resulting in the conclusion that a higher thermal conductivity equated to a lower surface temperature, lower wall superheat and better heat transfer performance. The current work disagrees with this finding noting copper to have the worst heat transfer performance compared with stainless steel and brass. At the onset of nucleate boiling, copper did have the lowest wall

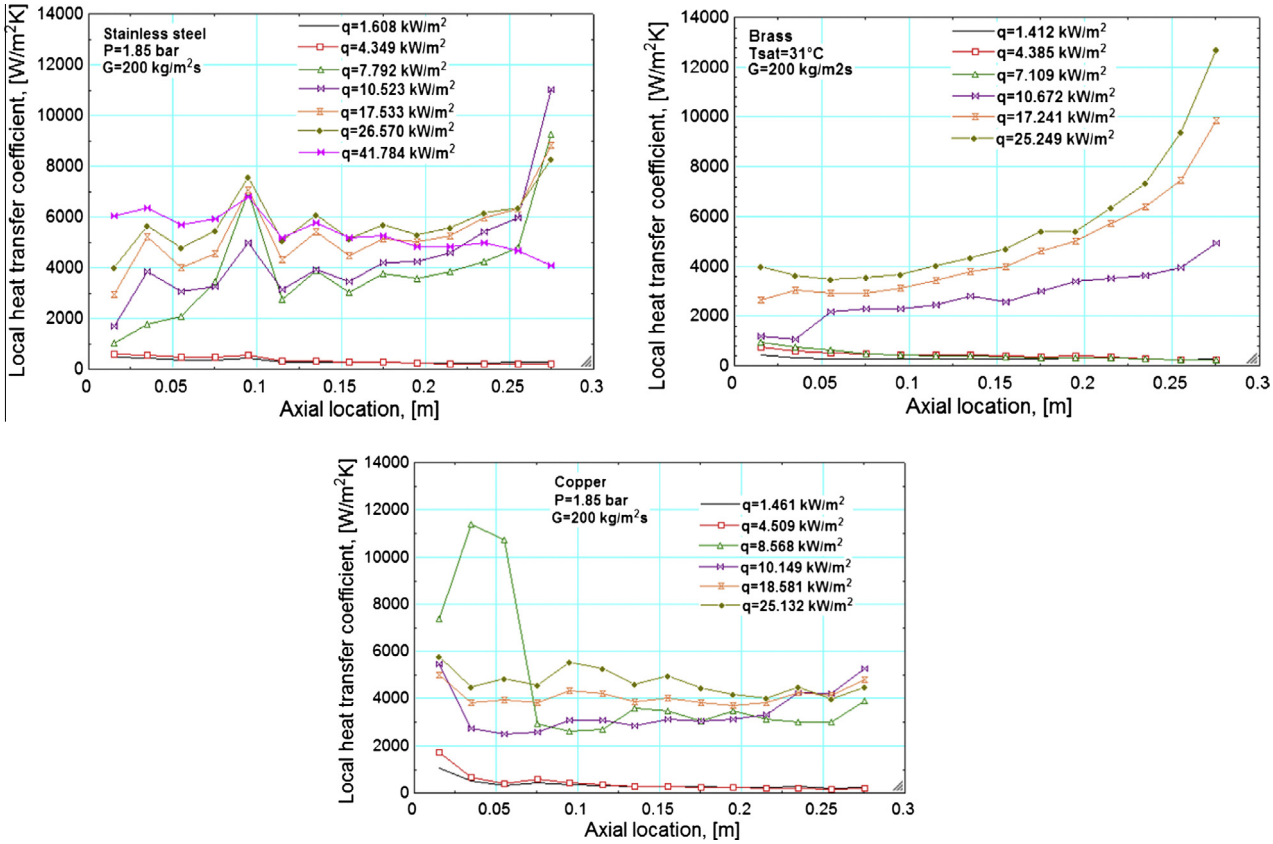

Fig. 20. Local heat transfer coefficient for stainless steel, brass and copper as a function of the axial location at an inlet pressure of 1.85 bar and mass flux of 200 kg/m^2 s.

superheat but stainless steel has the lowest superheat over the heat flux range hence disagreeing with [8]. At the same time, brass has a higher thermal conductivity than stainless steel but also a higher wall superheat. Furthermore, copper with the highest thermal conductivity resulted in wall superheat in the middle of the two tubes tested. Therefore, the present study indicates that the variation in thermal performance is not necessarily due to thermal conductivity differences but could be due to differences in surface characteristics. Further work may be necessary in this area.

Examination of Fig. 23 shows little effect of mass flux at a given heat flux for stainless steel and brass up to a vapour quality of 0.2. At $x > 0.2$, the mass flux effect is evident. However, when the heat transfer coefficient is plotted as a function of the axial location, see Fig. 24, there is no evidence of mass flux effect. These graphs also show that not only the magnitude but also the corresponding local vapour quality is similar for all mass fluxes for both tubes, i.e. at a mass flux of 200, the vapour quality is 0.44. It is not surprising that the vapour quality is similar as the flow patterns for each mass flux, at a heat flux of 17 kW/m^2, are the same. Copper shows no effect of mass flux, regardless of the vapour quality and irrespective of whether you examine Fig. 23 or Fig. 24. At a mass flux of 100 kg/m^2 s, the heat transfer coefficient is similar for all of the materials. At high heat fluxes, annular flow is evident for all materials. The flow patterns differ at low heat fluxes, with brass and copper having slug flow unlike stainless steel, which shows direct transition from single to annular flow with increasing heat flux.

The present results were compared with heat transfer correlations from the literature. The comparative results are included in

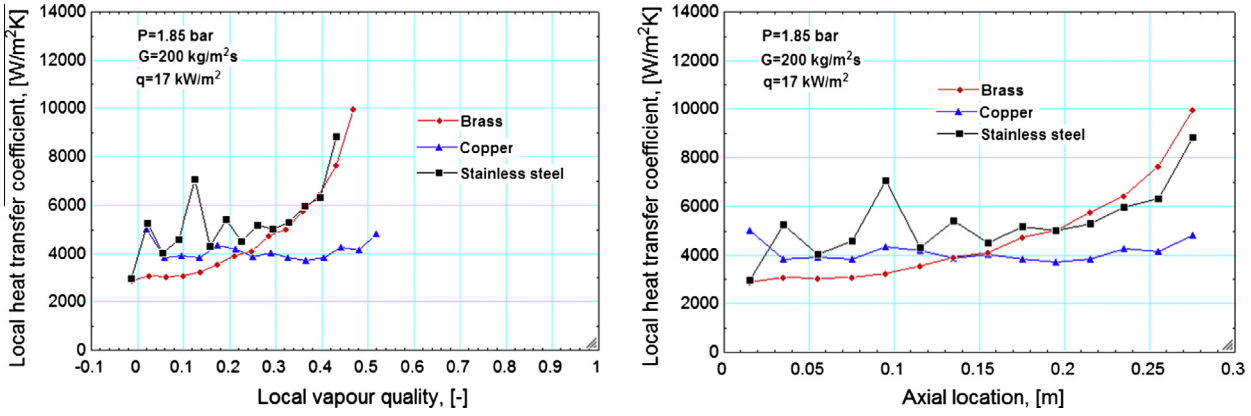

Fig. 21. Heat transfer coefficient for stainless steel, copper and brass at a heat flux of 17 kW/m^2.

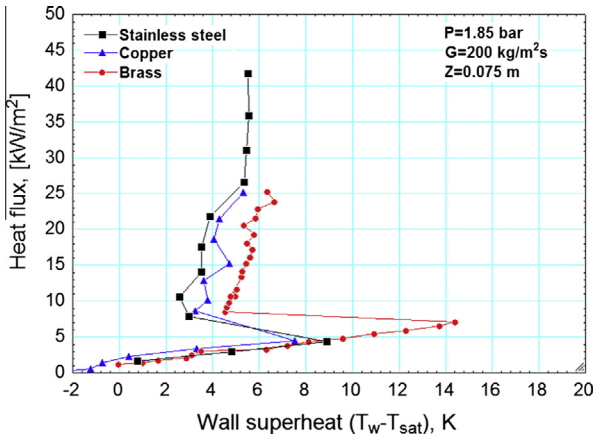

Fig. 22. Boiling curves for stainless steel, copper and brass.

Table 3 in terms of β and MAE. In these terms, the correlation of Mahmoud and Karayiannis [53] developed using R134a data, performed better for all three materials, although the comparison is considerably better for stainless steel and copper. Many of the correlations [54–57] do not include a vapour quality function and therefore give a constant value for the heat transfer coefficient with quality at each heat flux, Fig. 25. The other correlations, besides that of Kew and Cornwell [58], predict the heat transfer to decrease with increasing vapour quality, which is not seen in the results. As none of the correlations, besides that of Mikielewicz [56], include a function of surface characteristics, the same heat transfer coefficient is predicted for all three channels as the channel diameter and fluid is the same. The Mikielewicz [56] correlation uses the Cooper [59] correlation, as given below, for pool boiling which includes the *Rp* value but only accounts for a small part in the correlations, see Eq. (29). Note that the *Rp* value used for the Cooper [59] correlation is the old version, defined in DIN 4762/1:1960. The *Rp* value has since been redefined in the ISO standards [23]. Gorenflo [60] suggested the $Rp_{,old}$ value could be estimated from Eq. (28).

$$Rp_{,old} \approx 0.4\ Ra \tag{28}$$

$$h_{nb} = 55P_r^{0.12-0.4343lnR_p}(-0.4343lnP_r)^{-0.55}M^{-0.5}q^{0.67} \tag{29}$$

In general, the correlations perform better for the copper tube which does not have the sharp increase in heat transfer coefficient at high vapour qualities.

4. Conclusions

The main conclusions reached in this study are summarised below:

The structure of a surface defines the size and number of nucleation sites, which could affect the flow boiling patterns, pressure drop and heat transfer characteristics in a tube, especially as the diameter diminishes. The technique used in analysing a surface and processing the data could result in different surface data and this needs to be considered by the research community. The analysis of the stainless steel, copper and brass tubes through SEM and CFLM showed a difference in the structure of the surface. The same manufacturing process was used for all test sections, suggesting that the differences in the surface structure are due to the material. The average roughness, as well as other surface characteristics such as the maximum profile peak and maximum height, vary significantly between these surfaces.

For all three materials, the pressure drop was seen to increase with mass flux, although this is less evident with brass. The pressure drop for brass showed a steeper increase with increasing heat flux and also a higher magnitude of pressure drop for all mass fluxes. The floor distance to mean line (*Fp*), was very similar for

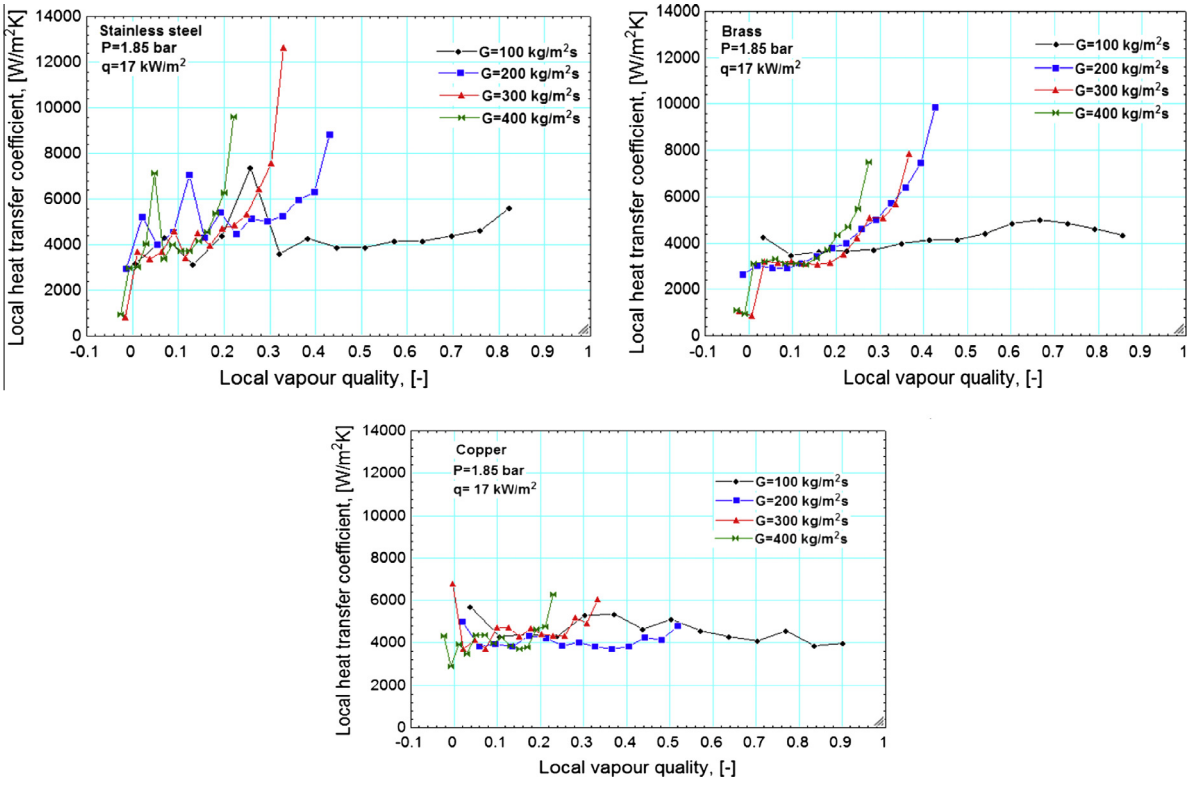

Fig. 23. Effect of mass flux on local heat transfer coefficient at a heat flux of 17 kW/m^2 and pressure of 1.8 bar for stainless steel, brass and copper.

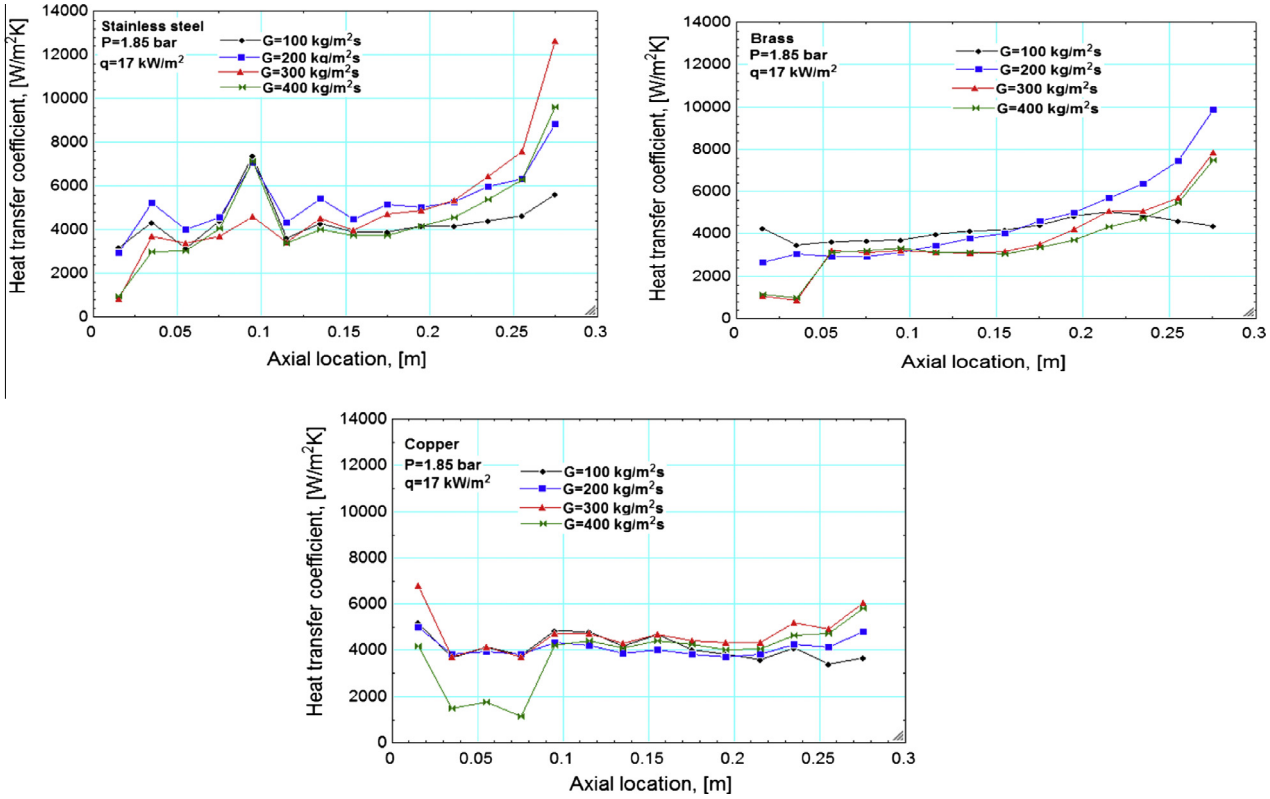

Fig. 24. Effect of mass flux on local heat transfer coefficient at a heat flux of 17 kW/m^2 and pressure of 1.8 bar for stainless steel, brass and copper as a function of axial location.

Table 3
Comparison with heat transfer correlations.

Correlation	Stainless steel		Brass		Copper	
	β %	MAE %	β %	MAE %	β %	MAE %
Lazarek and Black [54]	12.7	87.8	16.8	54.4	10.9	62.5
Tran et al. [55]	10.2	154.5	16.5	87.2	12.7	106.0
Li and Wu [61]	35.5	26.3	15.9	54.8	29.9	48.8
Mikielewicz [56]	41.7	26.2	25.5	32.8	35.0	38.3
Warrier et al. [46]	1.3	263.4	1.8	130.5	4.0	165.5
Kew and Cornwell [58]	16.5	89.9	16.6	70.1	12.4	58.4
Mahmoud and Karayiannis [53]	42.2	25.9	28.8	32.1	46.4	29.0
Mahmoud and Karayiannis [57]	32.2	36.3	28.7	20.5	28.0	16.3

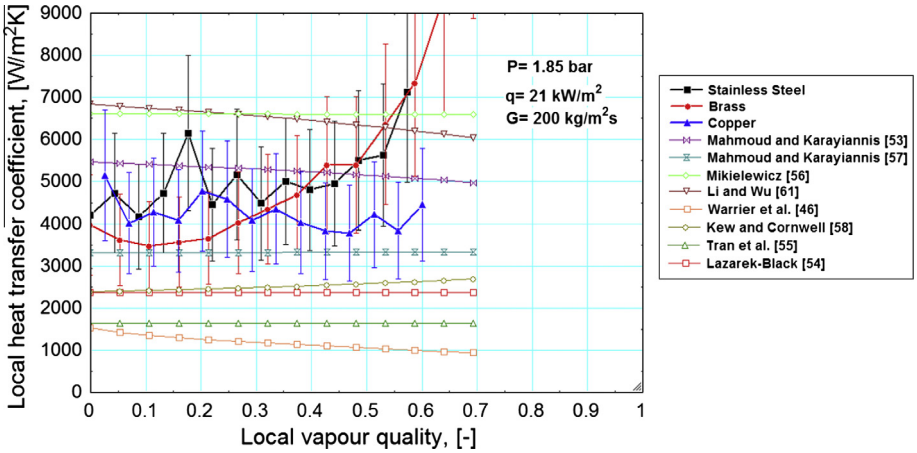

Fig. 25. Comparison of heat transfer correlations for copper, brass and stainless steel at P = 1.8 bar and G = 100 kg/m^2 s.

both stainless steel and brass but the pressure drops were vastly different, which was not inferred by the values of *Fp*. The *Fp* value was lowest for copper but this has a pressure drop in the middle of the other two materials.

The corresponding differences in the heat transfer coefficient in the stainless steel, brass and copper tubes appear to be smaller. Some differences are obvious however, namely the peaks in the profile of the heat transfer coefficient in the stainless steel tube, which could be due to different surface characteristics or surface flaws. There is no clear link between the surface roughness and the changes in the heat transfer coefficient, with the differences in the surface roughness being greater than the differences seen for the heat transfer coefficients. This interim conclusion, i.e. that the material itself does not have a significant effect on the heat transfer coefficient seems to concur with past reports in this area. However, the number of studies is small and we plan to continue testing within this field to aid in getting a final conclusion. In addition, it has been shown earlier that different manufacturing methods can produce significantly different surface characteristic and significantly different flow boiling heat transfer coefficients in small to micro tubes.

The correlations used, for both pressure drop and heat transfer, do not include any function of surface characteristics. There was limited success in comparing the present results for this fluid with pressure drop correlations. There was not one pressure drop correlation which performed best across the three materials. The heat transfer correlations proposed by Mahmoud and Karayiannis [53,57], performed better overall than the other heat transfer correlations for all materials. Further assessment of these relationships is currently underway with a larger databank.

Acknowledgments

The first author has a scholarship from the Thomas Gerald Grey Charitable Trust. The comments of Dr. J.S. Lewis are gratefully acknowledged. The comments of Dr. M. Mahmoud in the final preparation are also acknowledged.

References

[1] S.G. Kandlikar, Heat Transfer and Fluid Flow in Minichannels and Microchannels. Elsevier Ltd. first ed., 2006.
[2] T.G. Karayiannis, M.M. Mahmoud, D.B.R. Kenning, A study of discrepancies in flow boiling results in small to microdiameter metallic tubes, Exp. Thermal Fluid Sci. 36 (2012) 126–142.
[3] T.G. Karayiannis, D. Shiferaw, D.B.R. Kenning, Saturated flow boiling in small-to micro-diameter metallic tubes: experimental results and modelling, in: ECI Int. Conf. on Heat Transfer and Fluid Flow in Microscale, Whistler, 2008.
[4] Y. Liu, Multi-Phase Flow in Microchannels, Ph.D. thesis, University of Sydney, 2011.
[5] S.G. Kandlikar, P.H. Spiesman, Effect of surface finish on flow boiling heat transfer, in: Proceedings of the 1998 ASME International Mechanical Engineering Congress and Exposition, 1998, pp. 157–163.
[6] B. Jones, S.V. Garimella, Surface roughness effects on flow boiling in microchannels, J. Thermal Sci. Eng. Appl. 1 (4) (2009).
[7] T. Alam, P.S. Lee, C.R. Yap, Effects of surface roughness on flow boiling in silicon microgap heat sinks, IJHMT 64 (2013) 28–41.
[8] L. Zou, B.G. Jones, Heating surface material's effect on subcooled flow boiling heat transfer of R134a, Int. J. Heat Mass Transfer 58 (1–2) (2013) 168–174.
[9] A. Luke, Preparation, measurement and analysis of the microstructure of evaporator surfaces, Int. J. Therm. Sci. 45 (3) (2006) 237–256.
[10] D.J. Whitehouse, Handbook of Surface and Nanometerology, Taylor and Francis, second ed., 2011, p. 63.
[11] A.K. Bewoor, Metrology and Measurement, Tata McGraw-Hill Education, 2009. pp. 271–286.
[12] T.R. Thomas, Rough Surfaces, second ed., Imperial College Press, London, 1999.
[13] B. Griffiths, Manufacturing Surface Technology: Surface Integrity and Functional Performance. Penton 1857180291.
[14] E. Salek, The Handbook of Lubrication and Tribology: Theory and Design, CRC Press, 2012. 2001.
[15] H.S. Nielsen, Metrology Insight, vol. 3(1), Metrology Consulting, Inc., April 2000.
[16] B. Muralikrishnan, J. Raja, Computational Surface and Roughness Metrology, Springer, 2008.
[17] E. Oberg, F.D. Jones, H.L. Horton. Machinery's Handbook, 23rd ed., Industrial Pr, 1996.
[18] P.J. Ramón-Torregrosa, M.A. Rodríguez-Valverdem, A. Amirfazil, M.A. Cabrerizo-Vílchez, Factors affecting the measurement of roughness factor of surfaces and its implications for wetting studies, Colliods Surf. A 323 (2008) 83–93.
[19] S.G. Kandlikar, P.H. Spiesman, Effect of surface characteristics on flow boiling heat transfer, in: Eng. Foundation Conference on Convective and Pool Boiling, Germany, 1997.
[20] S.G. Kandlikar, D. Schmitt, Characterization of surface roughness effects on pressure drop in single-phase flow in microchannels, Phys. Fluids 17 (2005). 100606.
[21] Surface Texture, Surface Roughness, Waviness and Lay: ASME B46.1-2002, ASME, 2003.
[22] P.L. Young, T.P. Brackbill, S.G. Kandlikar, Comparison of roughness parameters for various microchannel surfaces in single-phase flow applications, Heat Transfer Eng. 30 (1–2) (2009) 78–90.
[23] Geometrical product specifications (GPS) surface texture: profile method-terms, definitions, and surface texture parameters. International Organization for Standardization, Geneva, Switzerland. 1997. BSENISO 4287:1998.
[24] B. Denkena, F. Hollmann, Process Machine Interactions: Prediction and Manipulation of Interactions between Manufacturing Processes and Machine Tool Structures, Springer, 2012.
[25] H, O'Hanley, Seperate Effects of Surface Roughness, Wettability and Porosity on Boiling Heat Transfer and Critical Heat Flux and Optimization of Boiling Surfaces. Thesis, MIT, 2012.
[26] X. Huo, L. Chen, Y.S. Tian, T.G. Karayiannis, Flow boiling and flow regimes in small diameter tubes, Appl. Therm. Eng. 24 (2004) 1225–1239.
[27] W. Qu, I. Mudawar, Flow boiling heat transfer in two phase micro-channel heat sinks-I. Experimental investigation and assessment of correlation methods, Int. J. Heat MassTransfer 46 (2003) 2755–2771.
[28] M.H. Maqbool, B. Palm, R. Khodabardeh, Investigation of two phase heat transfer and pressure drop of propane in a vertical circular minichannel, Exp. Therm. Fluid Sci. 46 (2013) 120–130.
[29] S. Bortolin, D. Del Col, L. Rossetto, Flow boiling of R245fa in a single circular microchannel, Heat Transfer Eng. 32 (13–14) (2011) 160–1172.
[30] H.W. Coleman, W.G. Steele. Experimentation and Uncertainty Analysis for Engineers, John Wiley, second ed., New York, 1999.
[31] S. Mostafa Ghiaasiaan, Convective Heat and Mass Transfer, Cambridge University Press, 2011.
[32] S.B. Choi, R.F. Barron, R.O. Warrington, Fluid Flow and Heat Transfer in Microtubes. DSC-Vol. 32, Micromechanical Sensors, Actuators, and Systems, ASME, 1991.
[33] R.K. Shah, A.L. London, Laminar flow forced convection in ducts, in: T.F. Irvin, J.P. Hartnett (Eds.), Advances in Heat Transfer, Academic, New York, 51–52, 124–128, 1978.
[34] T.M. Adams, S.I. Abdel-khalik, S.M. Jeter, Z.H. Qureshi, An experimental investigation of single phase forced convection in microchannels, Int. J. Heat MassTransfer 41 (6–7) (1998) 851–857.
[35] V. Gnielinski, New equations for heat transfer in turbulent pipe and channel flow, Int. Chem. Eng. 16 (1976) 359–368.
[36] B.S. Petukhov, Heat transfer and friction in turbulent pipe flow with variable physical properties, in: Advances in Heat Transfer, vol. 6, Academic Press, New York, 1970, pp. 503–564.
[37] F.W. Dittus, L.M.K. Boelter, Heat Transfer in Automobile Radiators of Tubular Type, Univ. California Berkeley, Publ. Eng. 2/13, 1930, pp. 443–461.
[38] J.C. Russ, The Image Processing Handbook, sixth ed., CRC Press, 2011.
[39] L. Chen, Y.S. Tian, T.G. Karayiannis, The effect of tube diameter on vertical two-phase flow regimes in small tubes, Int. J. Heat Mass Transfer. 49 (21–22) (2006) 4220–4230.
[40] E.A. Pike-Wilson, M.M. Mahmoud, T.G. Karayiannis, Flow boiling of R134a and R245fa in a 1.1 mm diameter tube, in: 11th International Conference on Nanochannels, Microchannels and Minichannels, Japan, 2013.
[41] R.W. Lockhart, R.C. Martinelli, Proposed correlation of data for isothermal two-phase two-component flow in pipes, Chem. Eng. Prog. (1949). 45-39.
[42] W. Zhang, T. Hibiki, K. Mishima, Correlations of two-phase pressure drop and void fraction in min-channel, Int. J. Heat Mass Transfer 53 (2010) 453–465.
[43] J.G. Collier, J.R. Thome, Convective Boiling and Condensation, third ed., Claredon Press, Oxford, 1996, p. 45.
[44] D. Del Col, A. Bisetto, M. Bortolato, D. Torresin, L. Rossetto, Experiments and updated model for two phase frictional pressure drop inside minichannels, Int. J. Heat MassTransfer 67 (2013) 326–337.
[45] K. Mishima, T. Hibiki, Some characteristics of air–water two-phase flow in small diameter vertical tubes, Int. J. Multiphase Flow 22 (4) (1996) 703–712.
[46] G.R. Warrier, V.K. Dhir, L.A. Momoda, Heat transfer and pressure drop in narrow rectangular channels, Exp. Therm. Fluid Sci. 26 (2002) 53–64.
[47] W. Qu, I. Mudawar, Measurement and prediction of pressure drop in two-phase microchannel heat sinks, Int. J. Heat Mass Transfer 46 (15) (2003) 2737–2753.
[48] W. Li, Z. Wu, A general correlation for adiabatic two-phase pressure drop in micro/mini-channels, Int. J. Heat Mass Transfer (53) (2010) 326–337.
[49] W. Yu, D.M. France, M.W. Wambsganss, J.R. Hull, Two-phase pressure drop, boiling heat transfer, and critical heat flux to water in a small-diameter horizontal tube, Int. J. Multiphase Flow 28 (2002) 927–941.

[50] P.-S. Lee, S.V. Garimella, Saturated flow boiling heat transfer and pressure drop in silicon microchannel arrays, Int. J. Heat Mass Transfer 51 (3–4) (2008) 789–806.
[51] S.G. Kandlikar, M.D. Cartwright, V.R. Mizo, A photographic study on nucleation characteristics of cavities in flow boiling, convective flow boiling, Taylor and Francis, 1996, pp. 73–3.
[52] K. Cornwell, R.D. Brown, Boiling surface topography, in: Proceedings of 6th International Heat Transfer Conference, Toronto, vol. 1, 1978, pp. 157–161.
[53] M.M. Mahmoud, T.G. Karayiannis, A statistical correlation for flow boiling heat transfer in micro tubes, in: Proceedings of the 3rd European Conference on Microfluidics–Microfluidics 2012, Heidelberg, 2012.
[54] G.M. Lazarek, S.H. Black, Evaporative heat transfer, pressure drop and critical heatflux in a small vertical tube with R-113, Int. J. Heat Mass Transfer 25 (7) (1982) 945–960.
[55] T.N. Tran, M.W. Wambsganss, D.M. France, Small circular- and rectangular channel boiling with two refrigerants, Int. J. Multiphase Flow 22 (3) (1996) 485–498.
[56] D.A. Mikielewicz, A new method for determination of flow boiling heat transfer coefficient in conventional-diameter channels and minichannels, Heat Transfer Eng. 31 (4) (2010) 276–287.
[57] M.M. Mahmoud, T.G. Karayiannis, Heat transfer correlation for flow boiling in small to micro tubes, Int. J. Heat Mass Transfer 66 (2013) 553–574.
[58] P.A. Kew, K. Cornwell, Correlations for the prediction of boiling heat transfer in small diameter channels, Appl. Therm. Eng. 17 (8–10) (1997) 705–715.
[59] M.G. Cooper, Saturation nucleate, pool boiling- a simple correlation, Int. Chem. Engng. Symp. 86 (1984) 785–792.
[60] D. Gorenflo, Pool Boiling, VDI Heat Atlas, VDI Verlag, Dűsseldorf, 1993.
[61] W. Li, Z. Wu, A general correlation for evaporative heat transfer in micro/minichannels, Int. J. Heat Mass Transfer (53) (2010) 1778–1787.